12-2016

Phase field simulations of plastic strain-induced phase transformations under high pressure and large shear

Mahdi Javanbakht
Isfahan University of Technology

Valery I. Levitas
vlevitas@iastate.edu, vlevitas@iastate.edu

Phase field simulations of plastic strain-induced phase transformations under high pressure and large shear

Abstract

Pressure and shear strain-induced phase transformations (PTs) in a nanograined bicrystal at the evolving dislocations pile-up have been studied utilizing a phase field approach (PFA). The complete system of PFA equations for coupled martensitic PT, dislocation evolution, and mechanics at large strains is presented and solved using the finite element method (FEM). The nucleation pressure for the high-pressure phase (HPP) under hydrostatic conditions near a single dislocation was determined to be 15.9 GPa. Under shear, a dislocation pile-up that appears in the left grain creates strong stress concentration near its tip and significantly increases the local thermodynamic driving force for PT, which causes nucleation of HPP even at zero pressure. At pressures of 1.59 and 5 GPa and shear, a major part of a grain transforms to HPP. When dislocations are considered in the transforming grain as well, they relax stresses and lead to a slightly smaller stationary HPP region than without dislocations. However, they strongly suppress nucleation of HPP and require larger shear. Unexpectedly, the stationary HPP morphology is governed by the simplest thermodynamic equilibrium conditions, which do not contain contributions from plasticity and surface energy. These equilibrium conditions are fulfilled either for the majority of points of phase interfaces or (approximately) in terms of stresses averaged over the HPP region or for the entire grain, despite the strong heterogeneity of stress fields. The major part of the driving force for PT in the stationary state is due to deviatoric stresses rather than pressure. While the least number of dislocations in a pile-up to nucleate HPP linearly decreases with increasing applied pressure, the least corresponding shear strain depends on pressure nonmonotonously. Surprisingly, the ratio of kinetic coefficients for PT and dislocations affect the stationary solution and the nanostructure. Consequently, there are multiple stationary solutions under the same applied load and PT, and deformation processes are path dependent. With an increase in the size of the sample by a factor of two, no effect was found on the average pressure and shear stress and HPP nanostructure, despite the different number of dislocations in a pile-up. The obtained results represent a nanoscale basis for understanding and description of PTs under compression and shear in a rotational diamond anvil cell and high-pressure torsion.

Disciplines

Aerospace Engineering | Condensed Matter Physics | Structures and Materials

Comments

This article is published as Javanbakht, Mahdi, and Valery I. Levitas. "Phase field simulations of plastic strain-induced phase transformations under high pressure and large shear." Physical Review B 94, no. 21 (2016): 214104. doi: 10.1103/PhysRevB.94.214104. Posted with permission.

Phase field simulations of plastic strain-induced phase transformations under high pressure and large shear

Mahdi Javanbakht[1] and Valery I. Levitas[2]

[1]*Department of Mechanical Engineering, Isfahan University of Technology, Isfahan 84156-83111, Iran*

[2]*Iowa State University, Departments of Aerospace Engineering, Mechanical Engineering, and Material Science and Engineering, Ames, Iowa 50011, USA*

(Received 19 May 2016; published 8 December 2016)

Pressure and shear strain-induced phase transformations (PTs) in a nanograined bicrystal at the evolving dislocations pile-up have been studied utilizing a phase field approach (PFA). The complete system of PFA equations for coupled martensitic PT, dislocation evolution, and mechanics at large strains is presented and solved using the finite element method (FEM). The nucleation pressure for the high-pressure phase (HPP) under hydrostatic conditions near a single dislocation was determined to be 15.9 GPa. Under shear, a dislocation pile-up that appears in the left grain creates strong stress concentration near its tip and significantly increases the local thermodynamic driving force for PT, which causes nucleation of HPP even at zero pressure. At pressures of 1.59 and 5 GPa and shear, a major part of a grain transforms to HPP. When dislocations are considered in the transforming grain as well, they relax stresses and lead to a slightly smaller stationary HPP region than without dislocations. However, they strongly suppress nucleation of HPP and require larger shear. Unexpectedly, the stationary HPP morphology is governed by the simplest thermodynamic equilibrium conditions, which do not contain contributions from plasticity and surface energy. These equilibrium conditions are fulfilled either for the majority of points of phase interfaces or (approximately) in terms of stresses averaged over the HPP region or for the entire grain, despite the strong heterogeneity of stress fields. The major part of the driving force for PT in the stationary state is due to deviatoric stresses rather than pressure. While the least number of dislocations in a pile-up to nucleate HPP linearly decreases with increasing applied pressure, the least corresponding shear strain depends on pressure nonmonotonously. Surprisingly, the ratio of kinetic coefficients for PT and dislocations affect the stationary solution and the nanostructure. Consequently, there are multiple stationary solutions under the same applied load and PT, and deformation processes are path dependent. With an increase in the size of the sample by a factor of two, no effect was found on the average pressure and shear stress and HPP nanostructure, despite the different number of dislocations in a pile-up. The obtained results represent a nanoscale basis for understanding and description of PTs under compression and shear in a rotational diamond anvil cell and high-pressure torsion.

DOI: 10.1103/PhysRevB.94.214104

I. INTRODUCTION

A. Interaction between PTs and plasticity at the microscale

Understanding of interaction between martensitic PTs and plasticity is one of the most fundamental problems in solid-solid PTs, see Ref. [1] and reviews [2–7]. Dislocational plasticity significantly changes PT thermodynamics, nucleation and growth kinetics, microstructure, and even the type of PT. For example, from one side, dislocations relax elastic stresses that appear due to heterogeneous distribution of the transformation strain, which promotes PT [2,4,6,8]. From the other side, dislocations produce an athermal threshold for interface propagation and can arrest the growth of martensite and lead to a morphological transition from plate to lath martensite [1,2,9]. This interaction is the basis for many applications in material science and technology. In particular, the transformation-induced plasticity phenomenon (see review [10]) can be used to obtain a desired combination of high strength and ductility in steels and ceramics [1]. Heat and thermomechanical treatments of materials are used for obtaining proper microstructure and physical properties.

At the microscale, PTs in elastoplastic materials were investigated in Refs. [3,11–14] using the principle of the minimum of Gibbs free energy (similar to PT in elastic materials) and sharp interfaces, while plasticity was described within continuum flow theory for an isotropic material. However, due to plastic dissipation and athermal interface friction, this principle cannot be applied to elastoplastic materials; interfaces are arrested before the energy minimum is reached. This problem was resolved in Refs. [15–19]. Utilizing the postulate of realizability [18–21], an extremum principle for determination of all nucleus parameters (like position, orientation, shape, and internal structure) was derived, which is applicable for elastoplastic materials and takes into account athermal interface friction. For thermally activated nucleation obeying Arrhenius-type kinetics, the principle of minimum of transformation time follows from the postulate of realizability [22].

Two different approaches were applied for determination of the driving force for the interface propagation. The Eshelby driving force (again, like for elastic materials) was utilized in Refs. [10,23–25]. Alternatively, in Refs. [9,19,26–28], the driving force was the dissipation increment due to PT only, which excludes plastic dissipation. Some contradictions of the first approach, which are not present in the second one, were found in Ref. [29]. Here, we will also address the problem of the driving force for interface propagation based on a nanoscale PFA. Since both transformation and plastic strains are quite large for many PTs, large strain formulation has been developed in Refs. [17,19] and applied to numerical

solutions of various problems, including nucleation and growth of martensite for thermally induced PT in steel [9], nucleation of martensite at the shear-band intersection for strain-induced PT in TRIP steel [30], and some other problems [27–29].

B. Phase field approach to interaction between PT and discrete dislocations at the nanoscale

For many problems, continuum plasticity is not an adequate model, and discrete dislocation plasticity should be included in consideration. Thus nucleation of the product phase occurs at stress concentrators caused by a group of dislocations, in particular, dislocation pile-up or tilt boundary [2,4], which is a typical nanoscale problem that cannot be described within continuum plasticity. Other dislocation configurations, like dislocation forest, produce athermal resistance to an interface motion. Also, while within continuum theory, plasticity does not violate coherency (i.e., continuity of displacements) of interfaces, at the nanoscale, nucleation of discrete dislocations leads to the loss of coherency of an interface, which changes its kinetics. In addition, with the development of nanoscience and technology, PT, and plasticity are studied in nanoparticles, films, and wires, and discrete dislocation plasticity is required. While there are some publications (e.g., Ref. [31]), which study interaction between sharp interfaces and dislocations, most of the efforts are within PFA.

PFA describes the nucleation and evolution of phase interfaces and dislocations with the help of the corresponding order parameters: η_i for PT from the austenite A ($\eta_i = 0$) to martensitic variant M_i ($\eta_i = 1$) and ξ_α for dislocations in the α slip system, where an integer part of ξ_α equals the number of complete dislocations. After choosing a proper thermodynamic potential, the evolution of phase and dislocation nanostructure is described by solution of the Ginzburg-Landau evolution equations for the order parameters. Both phase interfaces and dislocation cores have finite width, which is determined by the corresponding term in the potential related to the gradient of the order parameters.

In the paper, we will use the most advanced, from a mechanics point of view, PFA to multivariant martensitic PTs [32] and will apply it to a single martensitic variant. This theory is based on transformation strain related order parameters η_i and satisfies special conditions formulated in Refs. [33–35] for the description of typical experimental features of stress-strain curves for steels and shape memory alloys. In particular, $\eta_i = 0$ and $\eta_i = 1$ are the thermodynamically equilibrium values of the order parameters for *any stresses and temperature*. This allows one to use a consistent approximation of all material properties as functions of the order parameters, which for $\eta_i = 0$ and $\eta_i = 1$ coincide with known properties of A and martensitic variant M_i. This was not the case in the previous theories [36–39]. Also, PT criteria, which follow from the crystal lattice instability conditions, have a desired form in terms of the stress tensor and do not involve zero elastic moduli. The theory was generalized for large strains [32,40] and was applied for finite element solutions of various physical problems at small [41–44] and large strains [40,45].

The PFA to dislocations [46–53] is based on the representation of dislocation loops as thin martensitic inclusions (according to Nabarro [54]) and application (with some modifications) of PFA to martensite [36,37,46,47]. The PFA has appeared as a generalization of the Peierls-Nabarro dislocation model [55,56]. Transformation strain in this case is substituted with plastic strain, which represents a combination of simple shears along slip systems, characterized by the Burgers vector and normal to the slip planes. The order parameter for each slip system is related to the magnitude of the Burgers vector. Thus the order parameter for dislocation varies from $n-1$ to n when $n-1$ complete dislocations exist and the nth dislocation appears. The order parameter continuously describes the shear of one part of the crystal with respect to another by n Burgers vectors. In the classical discrete dislocation theory (sharp dislocations) [57,58], dislocation is defined as a boundary which separates a perfect lattice (or, in continuum formulation, material) and a lattice (material) slipped by an interatomic spacing (Burgers vector) along the slip plane. This definition is sufficient to derive all properties of dislocations and their interactions with external stresses and stress fields of other dislocations and other defects (e.g., point defects), including conservation of the Burgers vector and finding interaction forces between dislocations using solutions of the linear elasticity theory. In the PFA to dislocations [46–53], dislocations are introduced exactly in the same way as in traditional theory [57,58], i.e., by a slipping part of the crystal with respect to another by a Burgers vector within some region along the slip plane. Thus all main properties of dislocations (including conservation of the Burgers vector and stress field away from the dislocation lines, which determine the long-range interaction between dislocations and between external stresses and dislocations) are the same as in traditional theory [57,58]. In addition, the finite-width dislocation height and width of the dislocation core eliminate stress singularity and divergence of dislocation energy (like in the Peierls-Nabarro model [55,56]). This allows one, after proper calibration [47], to obtain reasonable results within the dislocation core and describe the short-range dislocation interaction. Instead of analytical solutions in traditional theory for stresses due to dislocations, which allow one to find forces between dislocations for some simple configurations [57,58], stresses in the PFA are found by a numerical solution of problems for an arbitrary distribution of the plastic strain, i.e., dislocations. In particular, these theories use spectral methods and the Khachaturyan microelasticity theory for an effective determination of the stress field and dislocation evolution for various physical problems [46–53]. These approaches are applicable for small strain linear elasticity only. The geometry of the dislocation lines is determined by a solution of the Ginzburg-Landau equations for the order parameters coupled to mechanics, similar to the geometry of the interfaces in the PFA for PTs. That is why specific geometric parameters of the dislocations (e.g., vector tangent to the dislocation line) are not explicitly present in the kinematic equation (2) and the expression for energy at each point (5)–(9). Similarly, the geometric parameters of phase interfaces are not explicitly present in the expressions for the transformation deformation gradient and energy. The geometric parameters are functionals of the entire solution.

These PFA formulations have the same deficiencies (and some others) as those for PFA for martensitic PTs. Most of these deficiencies have been eliminated in Refs. [35,59,60]

using approaches similar to those in Refs. [32,35] for martensitic PTs, as well as some other methods. In particular, a large-strain formulation was developed based on the multiplicative decomposition of the deformation gradient into elastic and plastic parts [Eq. (1)]. The relationship between the plastic strain and order parameters in small strain theory was substituted with the more general relationship (2) between the rate of the plastic deformation gradient and rates of the order parameters, which is consistent with the phenomenological crystal plasticity. Implementation of the thermodynamic equilibrium and stability conditions for homogeneous states led to the proper choice of the free energy [Eq. (8)] and the Burgers vector [Eq. (2)] versus the order parameters. This allowed us to reproduce a desired stress-order parameter curve and obtain a stress-independent equilibrium Burgers vector, as well as to eliminate nonphysical energy dissipation during elastic deformation. Also, a magnitude of the crystalline energy was defined as a periodic stepwise function of the coordinate along the normal to the slip plane [Eq. (8)], which determines the desired computational mesh-independent height of the dislocation bands. The gradient energy [Eq. (9)] includes an extra term, which prohibits the localization of the order parameter within a height smaller than the prescribed dislocation height, without producing an artificial interfacial energy. Nonperiodic boundary conditions for the order parameters are derived which include the change of the surface energy due to the exit of dislocations from the crystal [Eq. (21)]. The most complete theory for large strains and nonlinear elasticity was formulated in Ref. [60]. Nonlinear FEM procedure was developed and applied to various problems in Refs. [59,61].

A thermodynamically consistent PFA for the coupled PT and dislocation evolution at the nanoscale was developed in Ref. [62] as a synergistic combination of PFA for multivariant martensitic PTs [32] and dislocations [60] with nontrivial interactions. The interaction between PT and dislocations includes (a) the multiplicative kinematic decomposition of the deformation gradient into elastic, transformational, and plastic parts, (b) the inheritance of dislocations of A in M during martensitic PT and dislocations of M in A during reverse PT, as well as their further evolution along the nontraditional slip systems, (c) and dependence of all material parameters for dislocations on the order parameters that describe PT and additional contributions to the driving force for PT due to this dependence. An additional interaction between dislocations and PT occurs through stress fields generated by their eigenstrains and is determined by a solution of coupled PFA and mechanical problems. This theory was applied in Refs. [8,59,63,64] to solutions of some material problems, including revealing an athermal hysteresis which depends on the ratio of the phase interface width and the magnitude of the Burgers vector of a dislocation, finding a mechanism of semicoherent interface motion, dislocation inheritance by a propagating phase interface, and the temperature-induced nucleation, growth, and arrest of M plate in an A bicrystal. Some earlier PFAs on interaction of PTs and discrete dislocations include analytical [65] and numerical [66,67] solutions for M nucleation on dislocations, which were introduced through their stationary stress fields, or which belong to the moving phase interface only [68] and consequently do not involve phase field equations for dislocations and their inheritance during PT.

C. PTs under high pressure, compression, and shear

Application of high pressure to materials is a well-known way to discover new HPPs and phenomena. For example, high pressure leads to ionic boron [69], calcium carbides [70], highly energetic polymeric nitrogen [71] and CO_2 [72], as well as new superhard phases of carbon [73,74], BC_5 [75], 0B-BN [76], and BC_2N [77,78]. Multiple phases were predicted using first-principles simulations [79–83] but have not yet been confirmed experimentally. Some of these phases transform back during pressure release [71,72], which does not allow one to study their properties and use them in engineering applications. Transformation pressure for these phases is too high, which prevents their large-scale synthesis for engineering purposes. It is known from numerous experiments that superposition of large plastic shear in rotational Bridgman anvils [84] or a rotational diamond anvil cell (RDAC) [85–90,92,93,95,96] can lead to new phases that were not obtained under hydrostatic conditions and significantly reduces PT pressure. For example, a superhard phase IV of fullerene C_{60} [89,90] and single wall carbon nanotube [92] as well as highly energetic phases of nitrogen and sodium azide [86,87] were discovered under compression and shear in RDAC. A new high-density amorphous phase of SiC was observed *in situ* under pressure of 30 GPa and large shear [88] but no PTs were obtained under hydrostatic pressure up to 130 GPa. There are many examples that show that application of shear reduces PT pressure by a factor of 2 to 10 for some PTs [6,85,90,93,95–99,103], including PTs to superhard phases of BN [90,95], PTs in Si and Ge [85,96], and Zr and Zr-Nb alloys [97,98]. An important point is that some of these discoveries at relatively low pressure can be scaled up using high-pressure torsion [97–103] and ball milling [104–110].

A fundamental understanding of the physics responsible for such drastic reduction in PT pressure is far from being complete. Thus it was demonstrated [6,64,93] that a simple addition of the work of shear stress along the transformation shear strain to the macroscopic mechanical driving force (which is minus pressure times volumetric transformation strain) does not change transformation pressure significantly. This is because macroscopic shear stress is limited by the yield strength in shear ($\sim$1 GPa), which is small in comparison to the applied pressure, e.g., 10–50 GPa.

The fundamental difference between the plastic *strain-induced PTs under high pressure* and *pressure-induced or stress-induced PTs* was first formulated in Refs. [6,93]. Pressure-induced or stress-induced PTs initiate at pre-existing defects at stress below the yield strength, while plastic strain-induced PTs occur by nucleation at new defects (e.g., dislocation pile-ups) produced during plastic straining, which cause stronger stress concentrations than the pre-existing defects. This is why plastic strain-induced PTs require completely different thermodynamic and kinetic treatment and experimental characterization, which is coupled to the generation of defects and stress concentrators.

Despite numerous important and interesting experimental phenomena, the only analytical attempt to describe

strain-induced PTs under high pressure at the nanoscale has been a simple model of nucleation at the tip of a dislocation pile-up in infinite space [6,93]. Despite the simplicity and effective 1D treatment, this model explained many experimental results on PTs in DAC and RDAC and developed our intuition on the interaction between PTs and plasticity at the nanoscale. Due to the generic character of the model, qualitative conclusions from its application have been used by other groups to interpret their experimental findings in high-pressure torsion [99,103], mechanochemistry and ball milling [108–110], and shock-induced amorphization in Si [111].

It took ten years and multiple theoretical and algorithmic developments [32,40–45,59,63], as described above, before the PFA was prepared to be applied to the similar problem in Ref. [64]. A PFA was implemented to study PT at a dislocation pile-up in a nanograined bicrystal under uniaxial compression and shear with periodic boundary conditions at the lateral sides of a bicrystal [64]. The choice of a nanograined material is caused by the experimental observation that large plastic deformations under pressure lead to a nanograined structure [97,98,100–102], with a significant dislocation activity in grains. The study in Ref. [64] revealed some additional features which could not be obtained within an analytical model [6,93]. However, this was an exploratory study, and periodic boundary conditions are just one of the possibilities. Problem formulation in Ref. [64] considers the superposition of shear strain on a constrained uniaxial compression, even though the main discussion is on how shear reduces the PT pressure. In fact, the uniaxial compression reduces the PT pressure in comparison with hydrostatic conditions without shear, see, e.g., Refs. [91,94,96,99]. Alternative boundary conditions—free lateral surfaces—have been applied for an exploratory study of the shear-induced PT at zero pressure in Ref. [8]. Still, results obtained in Ref. [64], again due to their generic character, were applied in Ref. [103] for the interpretation of experiments on high-pressure torsion, in Ref. [112] on PTs in nanomaterials under mechanical loading, and in Ref. [111] on shock-induced amorphization in Si.

In the *current paper*, the general PFA for the interaction between PT and dislocation evolution developed in Ref. [62] is applied for comprehensive FEM simulations of the pressure and shear strain-induced PT to a HPP coupled to dislocation plasticity in a nanograin bicrystal. In contrast to Ref. [64], shear was superposed on equiaxial compression, which lead to results essentially different than in Ref. [64]. The main goal is to understand some generic features of how dislocations and PT compete with and assist each other and what coarse-grained parameters can characterize the overall behavior and allow to scale-up results for microscale. In particular, how under prescribed shear strain does a system relax stresses in terms of the number of dislocations in each grain and the concentration and morphology of the transformed region? Are dislocations generated in a low-(weaker) or high-(stronger) pressure phase or both, do they pass through phase interfaces and are they inherited by an alternative phase? What determines the stationary nanostructure and are unique or multiple nanostructures possible under the same conditions? Does back stress from PTs and plasticity in the right grain reduce the number of dislocations in the left grain? Answers to these questions and a comparison with the results in Ref. [64] for different boundary conditions will develop a deeper understanding and intuition for predicting the interaction between PTs and plasticity than we had based on previous papers [6,64,93]. While the main results are summarized in Abstract and Conclusions, here we mention the most unexpected findings. Thus, despite the very complex and heterogeneous stress distribution, plastic straining, and small sizes, the stationary morphology corresponds to the fulfillment of the simplest phase equilibrium condition, Eq. (22), for almost each point of the interface, which does not contain information about plasticity and interface energy. Moreover, the same phase equilibrium condition is approximately met in terms of stresses averaged over the entire grain or martensitic region. This is a conceptually important result due to two reasons: (1) it can be utilized for the development of a microscale description of strain-induced PTs and (2) it challenges previous wisdom [6,93] that phase equilibrium conditions do not enter the macroscopic (averaged) description of strain-induced PTs and cannot be determined from experiments for strain-induced PTs. Also, the major contribution to the transformation work is due to deviatoric stresses rather than pressure, while in previous works [6,93] the contribution of applied shear stresses to the transformation work was negligible.

The paper is organized as follows. In Sec. II, a complete system of the fully geometrically nonlinear equations for coupled PFA for single-variant PT, dislocation evolution, and continuum mechanics is formulated in the reference configuration and also simplified for a geometrically linear approximation. The problem formulation, material parameters, and numerical method are presented in Sec. III. Phase transformation under hydrostatic pressure is studied in Sec. IV. In Sec. V, PT and dislocation evolution in a nanograin bicrystal under several applied pressures and shear strains are studied with and without plasticity in the transforming grain. In Sec. VI, it is shown that the stationary high-pressure phase morphology and concentration can be described utilizing the local and averaged transformation work. The minimum shear and number of dislocations in a pile-up required for HPP nucleation were determined in Sec. VII. The effect of the ratio of the kinetic coefficients for PT and dislocation evolution on the intermediate and stationary nanostructure was discussed in Sec. VIII. Lack of the sample size effect in the interaction between phase transformation and dislocations was demonstrated in Sec. IX. Section X contains concluding remarks. Note that studies in Secs. VI–IX do not have a counterpart in Ref. [64] under periodic boundary conditions.

We designate vectors and tensors with boldface symbols and designate contractions of tensors $\boldsymbol{A} = \{A_{ij}\}$ and $\boldsymbol{B} = \{B_{ji}\}$ over one and two indices as $\boldsymbol{A}\cdot\boldsymbol{B} = \{A_{ij}B_{jk}\}$ and $\boldsymbol{A}:\boldsymbol{B} = A_{ij}B_{ji}$. The transpose of $\boldsymbol{A}$ is $\boldsymbol{A}^T$, $\boldsymbol{I}$ is the unit tensor; subscripts s and a mean symmetric and antisymmetric parts of a second-rank tensor, ∇ is the gradient operator with respect to an undeformed state, and $\otimes$ designates a dyadic product. Summation is assumed over the repeated indices.

II. COMPLETE SYSTEM OF EQUATIONS

In this paper, PTs between body centric cubic and body centric tetragonal lattices are considered in the examples.

In this case, slip systems of A (low-pressure phase, LPP) transform to the slip system of M (high-pressure phase, HPP) during PT. Since all equations are considered in the reference configuration, and slip systems of HPP are mapped back to LPP and coincide with the slip system of LPP, only a single set of the order parameters ξ_α is required, which characterizes slip along any slip systems of LPP and HPP, occurring either in LPP or HPP. Body forces are neglected and the surface energy is independent of phase and dislocations. We will utilize the theory for interaction between PTs and dislocations developed in Ref. [62] and the corresponding numerical approach presented in Ref. [8]. This theory synergistically combines fully geometrically nonlinear theory for martensitic PTs [32] and dislocations [60] and the corresponding numerical approaches presented in Refs. [45,61]. The complete system of equations from Refs. [8,62] is presented below. Also, for those who need to solve similar problems for infinitesimal strains, a simplified small strain version is presented as well.

1. Kinematics

I. Large strains

1.1. Multiplicative decomposition of the deformation gradient $\boldsymbol{F}$

$$\boldsymbol{F} = \boldsymbol{F}_e \cdot \boldsymbol{U}_t \cdot \boldsymbol{F}_p, \tag{1}$$

where $\boldsymbol{F}_e$ is the elastic, $\boldsymbol{U}_t$ is the symmetric transformation, and $\boldsymbol{F}_p$ is plastic contributions. In addition to the undeformed reference configuration Ω_0 and the deformed current configuration Ω, two intermediate stress-free configurations are introduced: Ω_t after elastic unloading from Ω to zero stresses and Ω_p after elastic unloading and reverse PT, respectively.

1.2. Rate of plastic deformation gradient

$$\begin{aligned}
\boldsymbol{l}_p &= \dot{\boldsymbol{F}}_p \boldsymbol{F}_p^{-1} = \sum_{\alpha=1}^{p} \frac{1}{H^\alpha} \boldsymbol{b}^\alpha \otimes \boldsymbol{n}^\alpha \dot{\Phi}(\xi_\alpha) \\
&= \sum_{\alpha=1}^{p} \gamma_\alpha \boldsymbol{m}^\alpha \otimes \boldsymbol{n}^\alpha \dot{\Phi}(\xi_\alpha), \quad \Phi(\xi_\alpha) = \phi(\bar{\xi}_\alpha) + \mathrm{Int}(\xi_\alpha); \\
\phi(\bar{\xi}_\alpha) &= \bar{\xi}_\alpha^2 (3 - 2\bar{\xi}_\alpha); \quad \bar{\xi}_\alpha = \xi_\alpha - \mathrm{Int}(\xi_\alpha),
\end{aligned} \tag{2}$$

where $\boldsymbol{b}^\alpha$ and $\boldsymbol{m}^\alpha$ are the Burgers vector of a dislocation in the αth slip system and corresponding unit vector, $\boldsymbol{n}^\alpha$ is the unit normal to the slip plane, ξ_α is the order parameter for a dislocation in the αth slip system, $\mathrm{Int}(\xi_\alpha)$ and $\bar{\xi}_\alpha$ are the integer and fractional parts of ξ_α, and $\gamma_\alpha = |\boldsymbol{b}^\alpha|/H^\alpha$ is the plastic shear for one dislocation within a dislocation band with the height H^α.

II. Small strains

$$\begin{aligned}
\boldsymbol{\varepsilon} &= (\boldsymbol{\nabla u})_s = \boldsymbol{\varepsilon}_e + \boldsymbol{\varepsilon}_t + \boldsymbol{\varepsilon}_p; \\
\boldsymbol{\varepsilon}_t &= \bar{\boldsymbol{\varepsilon}}_t \varphi(a, \eta_k); \\
\boldsymbol{\omega} &= (\boldsymbol{\nabla u})_a = \boldsymbol{\omega}_e + \boldsymbol{\omega}_t + \boldsymbol{\omega}_p; \\
\boldsymbol{\varepsilon}_p + \boldsymbol{\omega}_p &= \sum_{\alpha=1}^{p} \frac{1}{H^\alpha} \boldsymbol{b}^\alpha \otimes \boldsymbol{n}^\alpha \Phi(\xi_\alpha),
\end{aligned} \tag{3}$$

where $\boldsymbol{u}$ is the displacement vector, $\boldsymbol{\varepsilon}$ and $\boldsymbol{\omega}$ are the small strain and rotations, respectively.

1.3. Transformation-deformation gradient

$$\begin{aligned}
\boldsymbol{U}_t &= \boldsymbol{I} + \bar{\boldsymbol{\varepsilon}}_t \varphi(a, \eta) \\
\varphi(a, \eta) &= a\eta_k^2 (1 - \eta)^2 + (4\eta^3 - 3\eta^4); 0 < a < 6,
\end{aligned} \tag{4}$$

where η is the order parameter that describes PT from LPP ($\eta = 0$) to HPP ($\eta = 1$), $\bar{\boldsymbol{\varepsilon}}_t$ is the transformation strain of a HPP after complete PT, and a is a material parameter.

2. Helmholtz free energy per unit mass

$$\psi = J_t \psi^e + \psi_\eta^\theta + \psi_\xi^c + \psi_\eta^\nabla + \psi_\xi^\nabla; \quad J_t = \det \boldsymbol{U}_t. \tag{5}$$

2.1. Elastic energy

$$\rho_0 \psi^e = \tfrac{1}{2} \boldsymbol{E}_e : \boldsymbol{C} : \boldsymbol{E}_e; \quad \boldsymbol{E}_e = 0.5\left(\boldsymbol{F}_e^T \cdot \boldsymbol{F}_e - \boldsymbol{I}\right), \tag{6}$$

where ρ_0 is the mass density in the reference state, $\boldsymbol{E}_e$ is the elastic Lagrangian strain, and $\boldsymbol{C}$ is the forth-rank tensor of elastic moduli, which for simplicity is assumed to be equal for both phases.

2.2. Thermal energy

$$\begin{aligned}
\psi_\eta^\theta &= A\eta^2 (1 - \eta)^2 + \Delta G^\theta (4\eta^3 - 3\eta^4); \\
\Delta G^\theta &= -\Delta s\,(\theta - \theta_e), \quad A = A_0(\theta - \theta_c), \quad A_0 > 0,
\end{aligned} \tag{7}$$

where A and A_0 characterize the magnitude of the double-well barrier between LPP and HPP; ΔG^θ and Δs are the differences between the thermal part of the energy and entropy for HPP and LPP, respectively; θ_e is the phase equilibrium temperature for LPP and HPP for stress-free case; θ_c is the critical temperature at which stress-free LPP loses its thermodynamic stability.

2.3. Crystalline energy

$$\begin{aligned}
\psi_\xi^c &= \sum_{\alpha=1}^{p} \bar{A}_\alpha(\eta, \bar{y}^\alpha)(\bar{\xi}_\alpha)^2 (1 - \bar{\xi}_\alpha)^2; \\
\bar{A}_\alpha(\eta, \bar{y}^\alpha) &= A_\alpha^A + \left(A_\alpha^M - A_\alpha^A\right)\eta^2 (3 - 2\eta); \\
A_\alpha^{A,M}(y^\alpha) &= \begin{cases} \bar{A}_\alpha^{A,M} & \bar{y}^\alpha \leqslant H^\alpha; \\ k\bar{A}_\alpha^{A,M} & \bar{y}^\alpha > H^\alpha. \end{cases} \\
\bar{y}^\alpha &= y^\alpha - \mathrm{Int}\left(\frac{y^\alpha}{H^\alpha + w_\alpha}\right)(H^\alpha + w_\alpha); \quad k \gg 1,
\end{aligned} \tag{8}$$

where A_α^A and A_α^M are the magnitudes of the barriers in multiwell crystalline energy in LPP and HPP, respectively; y^α is the coordinate along the normal to the α_{th} slip plane; w_α is the width of the thin layer between dislocation bands, which is introduced with a much larger barrier than in a dislocation band ($k \gg 1$) in order to prevent spreading of a dislocation in the normal to slip plane direction; superscripts in $A_\alpha^{A,M}$ and similar terms mean that this parameter is defined either for A (LPP) or for M (HPP).

Equation (8) for the magnitude of the crystalline energy $A_\alpha^{A,M}(y^\alpha)$ is defined as a periodic stepwise function of the coordinate along the normal to the slip plane, which determines the desired height of the dislocation bands, H^α.

2.4. Gradient energies for PTs and dislocations

$$\psi_\eta^\nabla = \frac{\beta^\eta}{2}|\boldsymbol{\nabla}\eta|^2;$$

$$\psi_\xi^\nabla = 0.5\beta_\xi(\eta)\sum_{\alpha=1}^{p}((\nabla^m\xi_\alpha)^2 + Z(1-\bar{\xi}_\alpha)^2(\nabla^n\xi_\alpha)^2); \quad (9)$$

$$\beta_\xi(\eta) = \beta_\xi^A + \left(\beta_\xi^M - \beta_\xi^A\right)\eta^2(3-2\eta);$$

$$\nabla^m\xi_\alpha = \boldsymbol{\nabla}\xi_\alpha\cdot\boldsymbol{m}^\alpha; \quad \nabla^n\xi_\alpha = \boldsymbol{\nabla}\xi_\alpha\cdot\boldsymbol{n}^\alpha, \quad (10)$$

where the gradient energy coefficient β^η is for PT, and β_ξ^A and β_ξ^M are for dislocations in A (LPP) and M (HPP), respectively; Z is the ratio of the coefficients for the gradient energy normal to and along the slip plane; and superscripts m and n stand for the along $\boldsymbol{m}$ and $\boldsymbol{n}$, respectively. While for complete dislocation ($\bar{\xi}_\alpha \to 1$), the contribution of $\nabla^n\xi_\alpha$ disappears (as it should, because the crystal lattice is perfect after the dislocation passed, and it should not be penalized), presence of this term introduces a characteristic length along the normal to the slip system and eliminates the possibility of the problem being ill possed and the mesh-dependence of the numerical solution during formation of dislocation.

3. First Piola-Kirchhoff $\boldsymbol{P}$ and Cauchy $\boldsymbol{\sigma}$ stress tensor

I. Large strains

$$\boldsymbol{P} = \rho_0 J_t \boldsymbol{F}_e\cdot\frac{\partial\psi^e}{\partial\boldsymbol{E}_e}\cdot\boldsymbol{U}_t^{-1}\cdot\boldsymbol{F}_p^{T-1} = J_t\boldsymbol{F}_e\cdot\boldsymbol{C}{:}\boldsymbol{E}_e\cdot\boldsymbol{U}_t^{-1}\cdot\boldsymbol{F}_p^{T-1}; \quad (11)$$

$$\boldsymbol{\sigma} = J^{-1}\boldsymbol{P}\cdot\boldsymbol{F}^T = \rho J_t\boldsymbol{F}_e\cdot\frac{\partial\psi^e}{\partial\boldsymbol{E}_e}\cdot\boldsymbol{F}_e^T = \frac{1}{J_e}\boldsymbol{F}_e\cdot\boldsymbol{C}{:}\boldsymbol{E}_e\cdot\boldsymbol{F}_e^T; \quad (12)$$

$$J = \det\boldsymbol{F}; \quad J_e = \det\boldsymbol{F}_e; \quad J = J_eJ_t; \quad J_p = \det\boldsymbol{F}_p = 1, \quad (13)$$

where ρ is the mass density in the current configuration, and $J_p = 1$ due to plastic incompressibility. The equation for $\boldsymbol{\sigma}$ demonstrates why it was necessary to include J_t as a multiplier for the elastic energy in Eq. (5): it is based on tensors defined through the geometry of the current and elastically unloaded configurations only and does not contain info about Ω_p and Ω_0. Otherwise, the elasticity rule for M would depend on volumetric transformation strain for LPP → HPP PT, i.e., on the crystal lattice of LPP, which is contradictory.

II. Small strains and linear elasticity

$$\boldsymbol{\sigma} = \rho\frac{\partial\psi}{\partial\boldsymbol{\varepsilon}_e} = \boldsymbol{C}{:}\boldsymbol{\varepsilon}_e. \quad (14)$$

4. Ginzburg-Landau equations

4.1. The compact form in the reference configuration at large strains

$$\dot{\eta} = L^\eta X^\eta = L^\eta\left(\frac{1}{\rho_0}\boldsymbol{P}^T\cdot\boldsymbol{F}_e{:}\frac{\partial\boldsymbol{U}_t}{\partial\eta}\cdot\boldsymbol{F}_p + \boldsymbol{\nabla}\cdot\left(\frac{\partial\psi}{\partial\boldsymbol{\nabla}\eta}\right) - \frac{\partial\psi}{\partial\eta}\right);$$

$$\dot{\xi}_\alpha = L_\alpha(\eta)X_\alpha^\xi = L_\alpha(\eta)\left(\frac{1}{\rho_0}\tau_\alpha\gamma_\alpha\frac{\partial\Phi}{\partial\xi_\alpha} + \boldsymbol{\nabla}\cdot\left(\frac{\partial\psi}{\partial\boldsymbol{\nabla}\xi_\alpha}\right) - \frac{\partial\psi}{\partial\xi_\alpha}\right);$$

$$L_\alpha(\eta) = L_\alpha^A + \left(L_\alpha^M - L_\alpha^A\right)\eta^2(3-2\eta); \quad \tau_\alpha = \boldsymbol{n}^\alpha\cdot\boldsymbol{F}_p\cdot\boldsymbol{P}^T\cdot\boldsymbol{F}_e\cdot\boldsymbol{U}_t\cdot\boldsymbol{m}^\alpha, \quad (15)$$

where L^η is the kinetics coefficient for PT; L_α^A and L_α^M are the kinetics coefficients for dislocations in A and M, respectively; X^η and X^ξ are the thermodynamic driving forces conjugate to $\dot{\eta}$ and $\dot{\xi}_\alpha$, respectively; and τ_α is the resolved shear stress on the slip plane and in the slip direction for a dislocation.

4.2. Detailed form at large strains

$$\dot{\eta} = L^\eta\left\{\frac{1}{\rho_0}\boldsymbol{P}^T\cdot\boldsymbol{F}_e{:}\frac{\partial\boldsymbol{U}_t}{\partial\eta}\cdot\boldsymbol{F}_p - J_t\boldsymbol{U}_t^{-1}{:}\frac{\partial\boldsymbol{U}_t}{\partial\eta}\psi^e(\boldsymbol{E}_e,\eta) - J_t\frac{\partial\psi^e(\boldsymbol{E}_e,\eta)}{\partial\eta} - [2A\eta(1-\eta)(1-2\eta) + 12\Delta G^\theta\eta^2(1-\eta)]\right.$$
$$- \sum_{\alpha=1}^{p}\frac{\partial A_\alpha(\eta,\bar{y}^\alpha)}{\partial\eta}(\bar{\xi}_\alpha)^2(1-\bar{\xi}_\alpha)^2 - \sum_{\alpha,k=1}^{p}\frac{\partial A_{\alpha k}(\eta)}{\partial\eta}(\bar{\xi}_\alpha)^2(1-\bar{\xi}_\alpha)^2(\bar{\xi}_k)^2(1-\bar{\xi}_k)^2$$
$$\left. - 0.5\frac{\partial\beta_\xi(\eta)}{\partial\eta}\sum_{\alpha=1}^{p}\left((\nabla^m\xi_\alpha)^2 + Z(1-\bar{\xi}_\alpha)^2(\nabla^n\xi_\alpha)^2\right) + \beta^\eta\nabla^2\eta\right\}. \quad (16)$$

$$\dot{\xi}_\alpha = L_\alpha(\eta)\left\{\frac{6}{\rho_0}\tau_\alpha\gamma_\alpha\bar{\xi}_\alpha(1-\bar{\xi}_\alpha) + \frac{1}{2}\boldsymbol{\nabla}\beta_\xi(\eta)\cdot\boldsymbol{\nabla}\bar{\xi}_\alpha + \frac{1}{2}[Z(1-\bar{\xi}_\alpha)^2 - 1](\boldsymbol{\nabla}\bar{\xi}_\alpha\cdot\boldsymbol{n}^\alpha)(\boldsymbol{\nabla}\beta_\xi(\eta)\cdot\boldsymbol{n}^\alpha)\right.$$
$$+ \frac{1}{2}\beta_\xi(\eta)[\nabla^2\bar{\xi}_\alpha + (Z(1-\bar{\xi}_\alpha)^2 - 1)(\boldsymbol{\nabla}\cdot\boldsymbol{n}^\alpha)(\boldsymbol{\nabla}\bar{\xi}_\alpha\cdot\boldsymbol{n}^\alpha)] - 2Z(1-\bar{\xi}_\alpha)(\boldsymbol{\nabla}\bar{\xi}_\alpha\cdot\boldsymbol{n}^\alpha)^2$$
$$+ [Z(1-\bar{\xi}_\alpha)^2 - 1]\boldsymbol{\nabla}(\boldsymbol{\nabla}\bar{\xi}_\alpha\cdot\boldsymbol{n}^\alpha)\cdot\boldsymbol{n}^\alpha - 2A_\alpha(\eta,\bar{y}^\alpha)\bar{\xi}_\alpha(1-\bar{\xi}_\alpha)(1-2\bar{\xi}_\alpha)$$
$$\left. - 2A_{\alpha k}(\eta)\bar{\xi}_\alpha(1-\bar{\xi}_\alpha)(1-2\bar{\xi}_\alpha)(\bar{\xi}_k)^2(1-\bar{\xi}_k)^2 + \beta_\xi(\eta)Z(1-\bar{\xi}_\alpha)(\nabla^n\xi_\alpha)^2\right\}. \quad (17)$$

4.3. Small strains, linear elasticity

$$\dot{\eta} = L_\eta \left\{ \frac{1}{\rho_0}\boldsymbol{\sigma}:\frac{\partial \boldsymbol{\varepsilon}_t}{\partial \eta} - \frac{J_t}{2\rho_0}\left(\boldsymbol{I}:\frac{\partial \boldsymbol{\varepsilon}_t}{\partial \eta}\right)\boldsymbol{\varepsilon}_e:\boldsymbol{C}:\boldsymbol{\varepsilon}_e - [2A\eta(1-\eta)(1-2\eta) + 12\Delta G^\theta \eta^2(1-\eta)] \right.$$
$$- \sum_{\alpha=1}^{p} \frac{\partial A_\alpha(\eta,\bar{y}^\alpha)}{\partial \eta}(\bar{\xi}_\alpha)^2(1-\bar{\xi}_\alpha)^2 - \sum_{\alpha,k=1}^{p} \frac{\partial A_{\alpha k}(\eta)}{\partial \eta}(\bar{\xi}_\alpha)^2(1-\bar{\xi}_\alpha)^2(\bar{\xi}_k)^2(1-\bar{\xi}_k)^2$$
$$\left. - 0.5\frac{\partial \beta_\xi(\eta)}{\partial \eta}\sum_{\alpha=1}^{p}\left((\nabla^m \xi_\alpha)^2 + Z(1-\bar{\xi}_\alpha)^2(\nabla^n \xi_\alpha)^2\right) + \beta^\eta \nabla^2 \eta \right\}. \tag{18}$$

The Ginzburg-Landau equations for dislocations for the geometrically linear case do not differ from Eq. (17) but the expression for τ_α simplifies to $\tau_\alpha = \boldsymbol{n}^\alpha \cdot \boldsymbol{\sigma} \cdot \boldsymbol{m}^\alpha$.

5. Equilibrium equations

I. Large strains

$$\nabla \cdot \boldsymbol{P} = \boldsymbol{0}. \tag{19}$$

II. Small strains

$$\nabla \cdot \boldsymbol{\sigma} = \boldsymbol{0}. \tag{20}$$

6. Boundary conditions for the order parameters

$$\boldsymbol{n}_0 \cdot \nabla \eta = 0, \qquad \nabla \bar{\xi}_\alpha \cdot \boldsymbol{b}^\alpha = 0, \tag{21}$$

where $\boldsymbol{n}_0$ is the normal to the external surface in the reference configuration Ω_0. These conditions mean that during PT and when dislocations exist at the external surface, the surface energy does not change.

Since all material parameters for dislocations are different in LPP and HPP and change during the PT, they are interpolated with the same function $\phi(\eta) = \eta^2(3-2\eta)$, which satisfies the formulated in Ref. [32,35] properties: $\phi(0) = 0$, $\phi(1) = 1$, and $\phi'(0) = \phi'(1) = 0$. The η dependence of the dislocation parameters produces extra terms in the Ginzburg-Landau equation (16) for PT.

The comparison of the fully geometrically nonlinear and linearized small strain theories above demonstrates the main differences between these two theories. Namely, the geometrically nonlinear formulation uses exact multiplicative kinematic decomposition [Eq. (1)] and the more general relationship (2) between the rate of the plastic deformation gradient and rates of the order parameters, which is consistent with the phenomenological crystal plasticity; the Lagrangian elastic strain measure in the elastic energy [Eq. (6)] and elasticity rule [Eqs. (11)–(13); different stress measures in the elasticity rule, Eqs. (11)–(13). It also uses a more complex expression for the mechanical driving force in the Ginzburg-Landau equation for PT and dislocations [Eq. (15)], in particular, through a more complex expression for the resolved shear stress τ_α. Our approach utilizes all equations in the reference (underformed) configuration, including equilibrium equation (19) and all gradient operators. In addition, large displacements and change in geometry is taken into account, which is important for the problem under study.

III. PROBLEM FORMULATION AND COMPUTATIONAL APPROACH

A. Material parameters

The following parameters for PT and all slip systems have been used [8]: $A_\alpha = 0.894$ GPa for LPP, $A_\alpha = 2.68$ GPa for HPP, $L_\xi = 10^4$ $(\text{Pa s})^{-1}$, $L_\eta = 2600$ $(\text{Pa s})^{-1}$, $\beta_\xi = 4.36 \times 10^{-10}$ N, $Z = 0.05$, $H^\alpha = 1.4$ nm, $|\boldsymbol{b}| = 0.35$ nm, $\gamma = 0.25$, $a = 3$, $\theta_e = 215$ K, $\theta_c = -183$ K, $\theta = 298$ K; $k = 100$, and $w_\alpha = 0.1H^\alpha$. Parameters $A_0 = 22$ MPa K^{-1} and $\beta_\eta = 25.92 \times 10^{-10}$ N correspond to the phase interface energy of 1.12 J/m^2 and width of 1.0 nm.

For simplicity, an isotropic elasticity is utilized in Eq. (11) with a shear modulus $\mu = 71.5$ GPa and a bulk modulus $K = 112.6$ GPa for both phases. The above parameters correspond to the yield strength of LPP $\tau_A^c = A_\alpha^A/(a\gamma) = 1.2$ GPa and of HPP $\tau_M^c = A_\alpha^M/(a\gamma) = 3.6$ GPa, a phase equilibrium pressure $p_e = 3$ GPa, and a critical pressure for instability of the LPP $p_{cl} = 17.6$ GPa. The transformation strains are $\varepsilon_{tx} = \varepsilon_{ty} = -0.1$ and $\varepsilon_{txy} = 0.15$. We normalize the size, time, and stress parameters by 1 nm, 1 ps, and 1 GPa, respectively.

B. Geometry

A complete formulation should include consideration of a representative polycrystalline volume, which is approximately 1000 grains with different orientations, with at least 20–30 nm grain size. The PT from a cubic to tetragonal lattice contains three crystallographically equivalent variants of tetragonal lattice, each should be described with a separate order parameter. The body centric cubic lattice may have 48 (or a minimum of 12) crystallographically equivalent slip systems, each should also be described with a separate order parameter. This formulation is computationally prohibitive because it takes into account the complexity and strong nonlinearity of the system of equations under study and the necessity to resolve at the nanometer size the interface width and the dislocation core, which requires, at least, five-six finite elements for an accurate solution of the problem. We assume that the threshold for twinning in the tetragonal lattice is much higher than for slip and only one of the preferred crystallographic variants appears, but this is a small computational saving for a 3D formulation. Considering the 2D idealization in Ref. [64], which is similar to the accepted one below (Fig. 1), the minimum 3D configuration would include the same two grains but with a similar size in the third direction, which is orthogonal to the shear. An additional dimension and the inclusion of all slip systems increase the number of degrees of freedom by two orders of

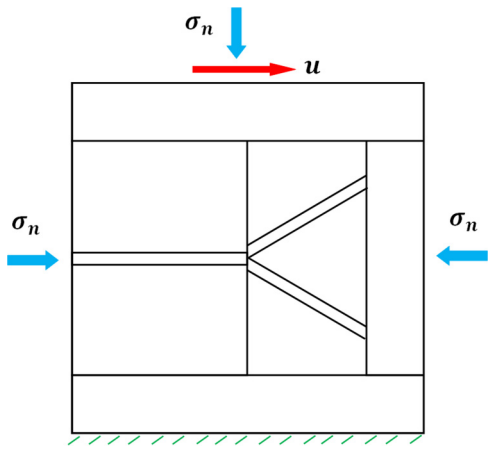

FIG. 1. Schematics of the sample loaded by normal stresses and shear.

magnitude as opposed to the 2D formulation used in Ref. [64] and below, which makes the parametric study impossible. In addition, increasing the number of slip systems makes it much more problematic to achieve convergence of solution due to the additional nonlinearities and their interactions. Still, a physical formulation for such a two-grain structure is not realistic in the third direction because of one grain in this direction. Since shear stresses in the direction orthogonal to the applied shear are much lower than those in the shear direction, the plastic strain in the third direction should be much smaller than that within the 2D plane. New nucleation sites are not expected because of this. Thus, as the best compromise between a physically adequate formulation and a computationally effective one, we consider the 2D formulation described below. It will allow us to focus on the main generic features of the interaction between PT and plasticity under pressure and shear.

We treat a square 60×60 sample, which is divided in the following regions (Fig. 1). (a) Left grain, a rectangular 30×40 region with a horizontal dislocation system in the middle, in which the mechanical and dislocation problems are solved but not the PT problem. (b) Right grain, a rectangular 20×40 region inside the sample with two dislocation systems, in which either all equations are solved or dislocation activity is excluded. (c) Two rectangular 60×10 regions at the top and the bottom, and a rectangular 10×40 region at the right side of the sample, in which only the mechanical problem is solved. They model elastic accommodation of the surrounding grains.

C. Boundary and initial conditions

In addition to Eq. (21) for the order parameters for the interaction of PT and the dislocations under plastic shear and pressure, the following boundary conditions are used for the mechanical problem: the lower side is fixed, the lateral and upper sides are subjected to normal homogeneous stress σ_n in the deformed state, and the upper side is also subjected to a homogeneous horizontal displacement u, which is given in terms of a prescribed macroscopic shear $\gamma = u/h$, where $h = 20$ is the height of the grains. As initial conditions, we accept perturbations $\eta = 0.01$ everywhere in the right grain, and $\xi_i = 0.01$ within each of slip systems; without perturbations, the evolution cannot start because $X^\eta = 0$ for $\eta = 0$ and $X^\xi_\alpha = 0$ for $\xi = 0$.

D. Numerical approach

We employed FEM and implemented the above system of equations in the COMSOL MULTIPHYSICS code to solve the coupled system of phase field and elasticity equations for cubic to tetragonal PT. Plane strain formulation and straight edge dislocations are used. All simulations are performed in the undeformed reference configuration; however, all results are mapped to and presented in the deformed state. As is usually assumed in 2D simulations [31,113] for cubic lattices, the slip directions are under 60° to each other. The backward time differentiation scheme is used for time integration with a time step of 10^{-2} fs. To reduce the number of the degrees of freedom and the computation time in comparison with linear finite elements, and also for improving convergence, quadrilateral finite elements with the quadratic polynomial for the shape function are utilized. Due to large geometric changes and to avoid mesh inversion and divergence of the solution, remeshing is applied automatically at some time steps. The time ranges during which remeshing is produced and the range of element sizes can be prescribed. Remeshing is performed only in local regions with strongly distorted elements, mostly near places with strong stress concentration and at the boundaries between different types of meshes. The accuracy of numerical solutions is confirmed in a number of ways summarized in Ref. [8].

IV. PHASE TRANSFORMATION UNDER HYDROSTATIC PRESSURE

To estimate the effect of shear on PT, first, it is necessary to determine the lowest pressure at which an HPP nucleus appears under hydrostatic conditions. Since, even for a heavily deformed material, the averaged distance between dislocations exceeds the size of the sample, we consider just one dislocation per two nanograins. First, we create one dislocation in the left grain by applying shear displacement $u = 1.4$ at the upper edge without any pressure on either side, and we arrest it at the grain boundary by stopping to solve the Ginzburg-Landau equation for dislocations. Then, the applied shear stress is reduced to zero, producing a stress-free sample with a single dislocation. After this, all mechanical boundary conditions are substituted with homogeneous stresses (pressure) normal to the deformed surface. It was found that the lowest pressure at which the nucleus appears is $p_h = 15.9$, after which it grows and fills a major part of the grain (Fig. 2). This is reasonable, because 15.9 is significantly higher than $p_e = 3$, which determines the local interface propagation pressure. Still, PT is not completed because the pressure in the transformed region and at the interface is reduced below p_e due to the transformation volume reduction. Thus one dislocation reduces the pressure required to nucleate HPP from $p_{cl} = 17.6$ by 10%, but it is still much higher than p_e.

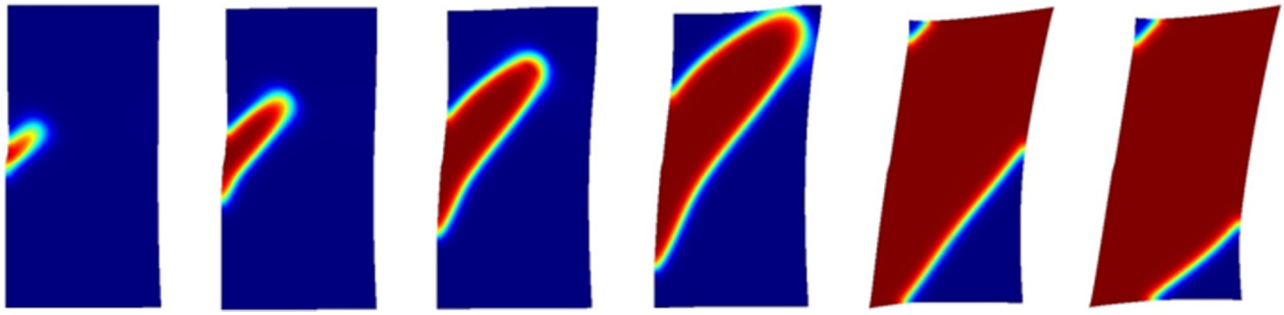

FIG. 2. Evolution of high-pressure phase under the hydrostatic pressure of 15.9 in the presence of a single dislocation.

V. PHASE TRANSFORMATION IN A NANOGRAINED MATERIAL UNDER COMPRESSION AND SHEAR

A. Dislocation evolution

We consider three different external pressures $p = \sigma_n = 0$, 1.59 (10% of p_h), and 5 (32% of p_h). This will allow us to elucidate the significant effect of stress concentration created by dislocations on the nucleation of HPP at pressures much below p_h. First, we apply the chosen normal stresses at the lateral and upper sides of the sample and then the homogeneous horizontal displacement u at the upper side. Initially, we solve the mechanical problem in the entire sample and the dislocation evolution problem in the left grain only. Under prescribed pressure and shear, several dislocations nucleate from the grain boundary one after another and move to the left side. Some of these dislocations leave the sample at the free surface, creating a step. Other dislocations densely pile-up at the grain boundary, creating a strong concentration of the stress tensor near the pile-up tip.

Figure 3 presents the evolution of dislocations in the left grain. As it is customary, a dislocation sign indicates the slip plane and the extra half-plane of atoms creating a dislocation. Under prescribed $\gamma = 0.35$, six dislocations appear in the left grain. As can be seen, a couple of the first positive and negative dislocations nucleate near the grain boundary creating a step. Then, a negative dislocation propagates to the left to the sample surface. The next dislocation couples nucleate near the grain boundary or in the middle of the dislocation band. Positive dislocations propagate to the right, four of which create a step at the grain boundary, and two of which are piled up near the grain boundary. Negative dislocations move to the left, five of which create a step at the left sample surface and only one piles up near the sample surface. A dislocation pile-up creates stress concentration near its tip. This leads to the increase in the local thermodynamic driving force for PT to HPP in the region near the dislocations tip in the right grain, which causes HPP nucleation. We will determine, for each applied pressure, the least number of dislocations in the left grain required for nucleation of HPP. In fact, the initial perturbation $\eta = 0.01$ in the right grain will disappear for less than the specified number of dislocations in the left grain.

The equal distance between a number of dislocations in a pile-up near the grain boundary in Fig. 3 and in most of figures below looks contradictory at first glance, because a known analytical solution gives increasing spacing for dislocations away from the head dislocation [57]. However, the analytical solution is valid for small strains (and, consequently, stresses) and a distance between dislocations exceeding dislocation core width, as well as for infinite space, i.e., our results are well beyond of the applicability of this solution. The main reasons for the difference between our solution and the analytical one are as follows. (a) Geometric changes leading to the appearance of steps at the grain boundaries, in which the distance between dislocations must be equal to the Burgers vector. Steps should be excluded from comparison with analytical solution completely. (b) At small spacing, the repulsion force between dislocations grows drastically due to interaction of dislocation cores through the gradient energy. Stresses acting on dislocations are so high that dislocations can be equilibrated by strong core interactions only. This leads to (almost) the same spacing between dislocations. (c) Large strains (=0.35) are inconsistent with the small strain and linear elastic solution. (d) There is stress relaxation outside the double pile-up due to the small size of the sample and relaxation processes in the right grain. Note that due to some of the deviations of reality from the conditions for the analytical solution, even for much smaller stresses and larger grains,

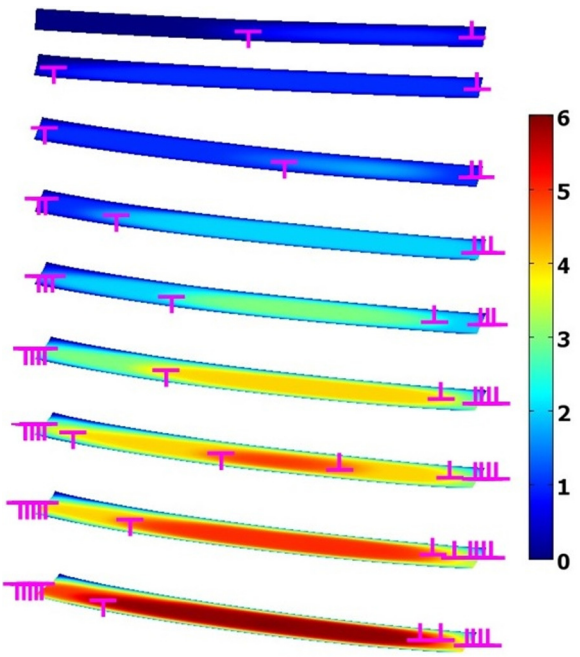

FIG. 3. Evolution of dislocations in the left grain under prescribed shear $\gamma = 0.35$ and $\sigma_n = 0$.

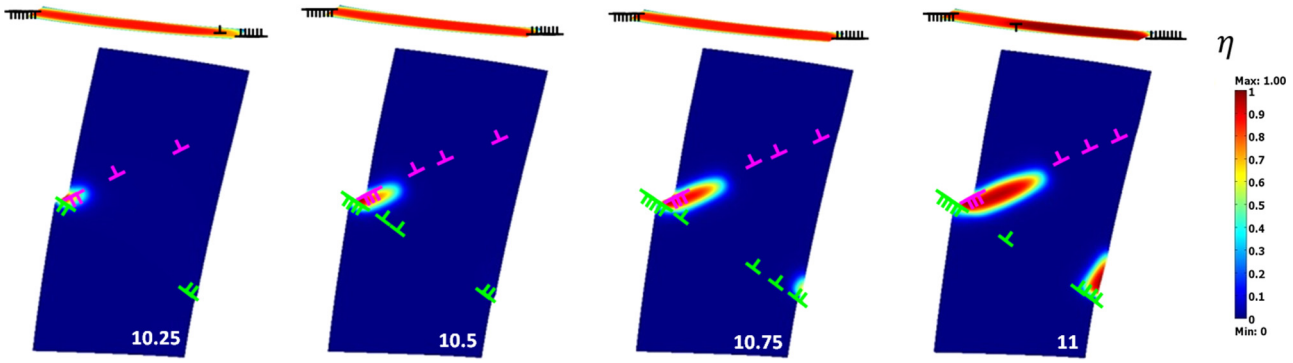

FIG. 4. Evolution of the high-pressure phase and dislocations for some initial stages under $p = 0$ and $\gamma = 0.3$ with plasticity in the right grain. The evolution of dislocations in the left grain is shown at the top.

spacing between the first dozen of dislocations near an obstacle is approximately the same, see e.g., Fig. 21-3 in Ref. [57].

Next, we allow PTs and plasticity (two $\pm 30^\circ$ inclined dislocations) in the right grain. The reason why we first create some dislocations in the left grain before allowing PTs and plasticity in the right grain is the same as above: if the stress concentration is not large enough at the pile-up tip, the initial perturbations $\eta = 0.01$ and $\xi_i = 0.01$ disappear and do not grow for any larger shear. Moreover, due to the competition between PTs and dislocations, stresses could be relaxed by nucleation of dislocations, and the initial HPP would disappear, so a further increase in shear will promote plasticity only and increase the number of dislocations, while PTs will not start due to the zero initial conditions. For each pressure, we increase the shear by increasing the applied displacement until we obtain the first nucleation of HPP. This reveals the least number of dislocations required to nucleate HPP under the prescribed pressure and shear with plasticity in the right grain. Also, the evolution of dislocations and HPP and the stationary nanostructure will be presented.

B. Phase transformation at zero applied pressure

For zero pressure, the first nucleation of HPP and dislocation in the right grain occur for shear $\gamma = 0.3$, creating eight dislocations in the left grain. Their evolution is presented in Fig. 4 for some initial stages. While the dislocations and HPP nucleus evolve in the right side, the number of dislocations in the left grain does not change. For the lower shear $\gamma = 0.2$, four dislocations are generated in the left grain and induce dislocations in the right grain, but no HPP appears. The main impressive result here is that in a nanograined material PT to HPP with $p_h = 15.9$ and $p_e = 3$ can occur without external pressure, just under shear stresses and internal stresses due to dislocation pile-up.

C. Phase transformation at $p = 1.59$

1. Evolution of dislocation and phase structures

For the pressure $p = 1.59$, the first HPP nucleation occurs for shear 0.35, which creates 7 dislocations in the left grain. The evolution of the HPP phase and dislocations is presented in Fig. 5 until the stationary solution is reached. In contrast to the problem without pressure, while the HPP nucleus in the right grain grows, the number of dislocations increases in both grains. For the lower shear $\gamma = 0.3$, 7 dislocations are generated in the left grain, which induce dislocations in the right grain without HPP at the left grain boundary but with a small HPP nucleus at the intersection of the dislocations and the right grain boundary [Fig. 6(a)]. Note that if plasticity is disallowed in the right grain, *HPP nucleation happens at much lower shear of* $\gamma = 0.21$ *resulting in three dislocations in the left grain* [Fig. 6(b)]. This emphasizes the significant role of plasticity in the transforming grain for stress relaxation, which competes with PT and *nucleation of HPP*. The evolution of the HPP phase and dislocations in the left grain for the shear $\gamma = 0.35$ but without plasticity in the right grain is represented in Fig. 7. The HPP growth is faster without plasticity in the right grain, because PT is the only stress relaxation mechanism. Also, at intermediate transformation stages, HPP nucleates in the lower right corner of the right grain but later disappears. The number of dislocations in the left grain for the problem with PT and plasticity increases faster than without plasticity.

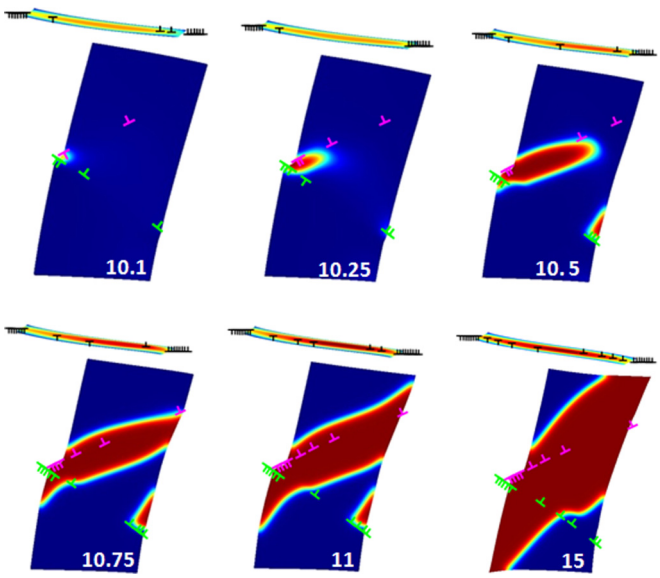

FIG. 5. Evolution of the high-pressure phase and dislocations under $p = 1.59$ and $\gamma = 0.35$ with plasticity in the right grain.

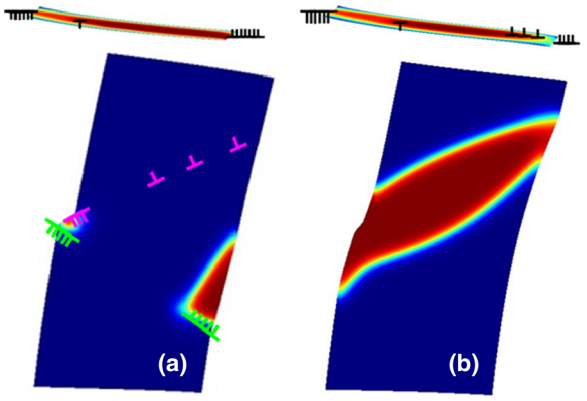

FIG. 6. High-pressure phase morphology and dislocation structure at $t = 10.75$ for $p = 1.59$ and $\gamma = 0.3$ with (a) and without plasticity (b).

2. *Concentration of the high-pressure phase*

The concentration of the HPP c is defined as the ratio of the transformed area to the grain area $\mathcal{S}_0$ in the undeformed state as $c = \int \eta dV_0/V_0 = \int \eta d\mathcal{S}_0/\mathcal{S}_0$. The plot of the concentration of HPP c versus time in Fig. 8 demonstrates that concentration is higher for the case without plasticity than with plasticity in the right grain. This is because plasticity in the right grain competes with PT as the stress relaxation mechanism. Plasticity reduces stress concentrators due to dislocation pile-up in the left grain. While stress concentration is still sufficient for nucleation, stresses away from it reduce, which suppresses PT. However, the *effect of plasticity in the transforming grain on stationary concentration c is much weaker than on nucleation*. Thus, without plasticity, the stationary value $c = 0.8$ is 5% higher than with plasticity.

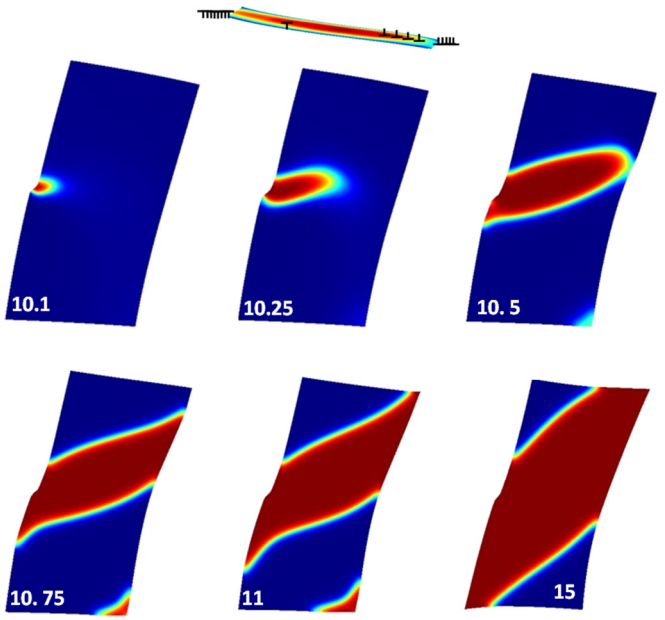

FIG. 7. Evolution of the high-pressure phase under $p = 1.59$ and $\gamma = 0.35$ without plasticity in the right grain for dislocation structure in the left grain shown on the top.

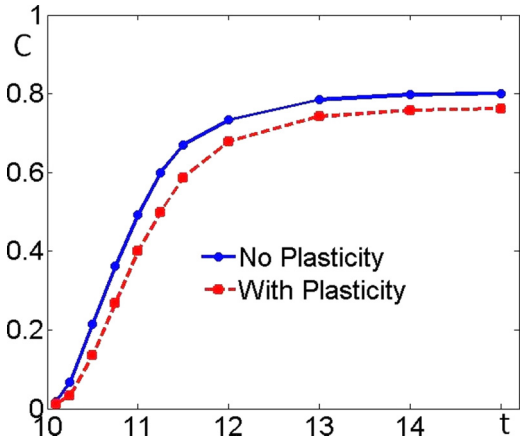

FIG. 8. Phase concentration vs time for $p = 1.59$ and $\gamma = 0.35$ with and without plasticity in the right grain.

During evolution after the concentration reaches some small value, it linearly increases with time until it reaches $c = 0.5$ with plasticity and $c = 0.6$ without plasticity. For larger time, c increases gradually until it reaches the stationary solution. The difference between concentrations for both cases reduces after $t = 11.5$ (as will be seen later, this time corresponds to the maximum transformation work) and becomes almost constant. The reason is that, due to the larger kinetic coefficient for dislocation evolution, dislocations are generated and reach a stationary configuration faster than the HPP, so they suppress PT stronger at the initial stages. However, the stationary dislocations, which did not reach the surface and stayed inside the grain, in particular dislocations belonging to the -30° inclined slip system, still suppress PT and result in an almost constant difference in concentrations of HPP.

3. *Averaged pressure and shear stress*

The averaged pressure $\bar{p} = -0.5(\bar{\sigma}_x + \bar{\sigma}_y)$ and shear stress $\bar{\tau}$ over the right grain are plotted versus time and also versus concentration in Figs. 9 and 10, respectively. After the concentration reaches some small value, $\bar{p}$ linearly decreases in time until $t = 11.5$, and then gradually decreases until it reaches the stationary value. The pressure $\bar{p}$ at each time step for the case without plasticity is lower than that of the case with plasticity, and their difference increases with time. This

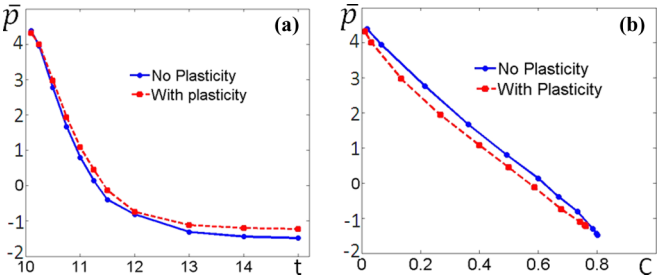

FIG. 9. Pressure averaged over right grain vs time and the concentration of high-pressure phase under $p = 1.59$ and $\gamma = 0.35$ in the right grain with and without plasticity. With plasticity, the pressure is higher for the same time but lower for the same concentration of high-pressure phase.

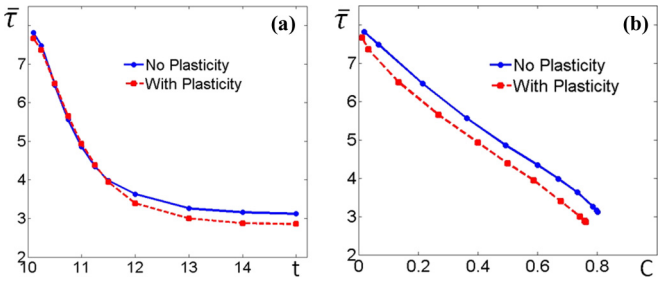

FIG. 10. Shear stress averaged over right grain vs time and concentration of high-pressure phase under $p = 1.59$ and $\gamma = 0.35$ in the right grain with plasticity and without it.

is due to the larger transformed region, which causes a larger reduction in volume, resulting in lower pressure. However, $\bar{p}$ for the case without plasticity is higher than that of the case with plasticity for the same concentration of HPP (Fig. 10). This is reasonable because even though the same concentration of HPP corresponds to the same reduction in volume, there is additional relaxation due to dislocation generation, which reduces pressure as well. For both cases, $\bar{p}$ linearly decreases with concentration with almost the same slope.

The averaged shear stress $\bar{\tau}$, after the concentration reaches some small value, linearly decreases with time until $t = 11.5$, and then it gradually decreases until it reaches the stationary value, similar to the averaged pressure. The shear stresses $\bar{\tau}$ with and without plasticity in the right grain are practically the same for $t < 11.5$; later, their difference increases with time. In contrast to $\bar{p}$, stress $\bar{\tau}$ without plasticity is higher than with plasticity for the same time and concentration. This is because of additional relaxation of shear stresses with the appearance of dislocations and motion in the right grain while additional volume reduction does not affect shear stresses significantly. Similar to $\bar{p}$, shear stress $\bar{\tau}$ linearly decreases with concentration with almost the same slope for both cases.

The key points in these results are the following. (a) Before PT, due to dislocation pile-up as well as the small size of the grains, not only the local but also the averaged pressure over the right grain drastically increase from the average pressure over the entire sample $\bar{p} = 1.59$ to 4.46. Similarly, the average shear stress over the grain increases from the average shear stress over the entire sample $\bar{\tau} = 5.83$ to 7.85.

(b) During PT, pressure drops to zero and then becomes tensile with the maximum magnitude of -1.43. The reason is the large volume reduction due to PT. While shear stress relaxes due dislocation activity and PT, its stationary value is 3, i.e., is quite large. This is a manifestation of the grain-size dependence of the yield strength due to the limited number of dislocations that can appear within small grains. Also, the yield strength increase from $\tau_A^c = 1.2$ in LPP to $\tau_M^c = 3.6$ in HPP, which occupies the major part of the transforming grain.

D. Phase transformation at $p = 5$

1. Dislocation and phase structures

For the pressure $p = 5$, the first HPP nucleation occurs near the tip of the dislocation pile-up at shear $\gamma = 0.3$ creating 6 dislocations. The evolution of the HPP and dislocations is

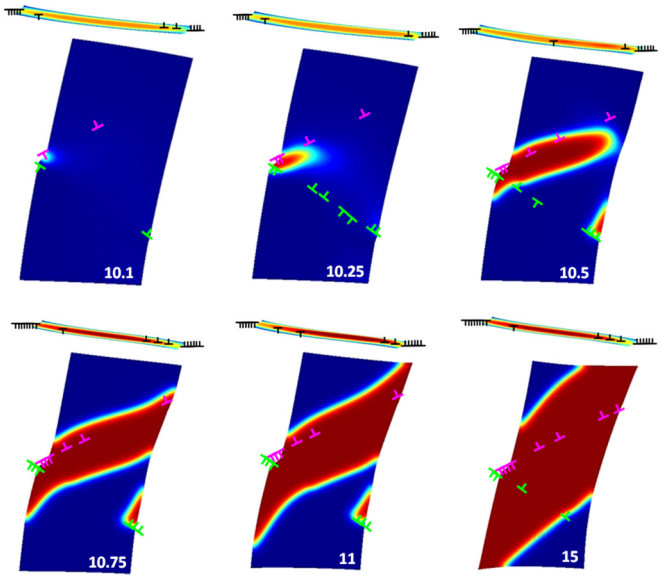

FIG. 11. Evolution of the high-pressure phase and dislocations under $p = 5$ and $\gamma = 0.3$ with plasticity in the right grain.

presented in Fig. 11 until the stationary solution is reached. During growth of HPP region, the number of dislocations in both grains increases. Nucleation starts from two places. However, the HPP region at the intersection of dislocations and the right grain boundary disappears (similar to the problem at $p = 1.59$), but in contrast to the case at $p = 1.59$, dislocations move back from the right boundary and one pair of dislocations disappears. In the absence of plasticity in the right grain, the nucleation and evolution occur from a single place; however, the stationary nanostructure is not much different from that with plasticity (Fig. 12). Also, for the lower shear $\gamma = 0.25$, four dislocations in the left grain are generated, causing dislocation nucleation within the $\pm 30^\circ$ inclined slip systems in the right grain, but HPP appears at the intersection of the

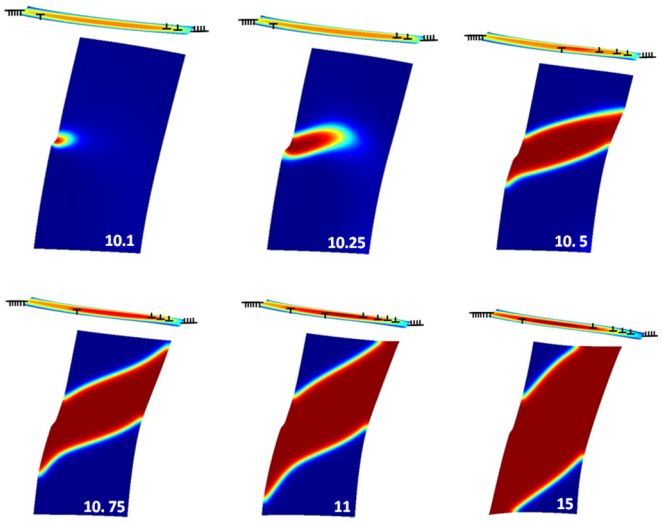

FIG. 12. Evolution of the phase and dislocations under $p = 5$ and $\gamma = 0.3$ without plasticity in the right grain.

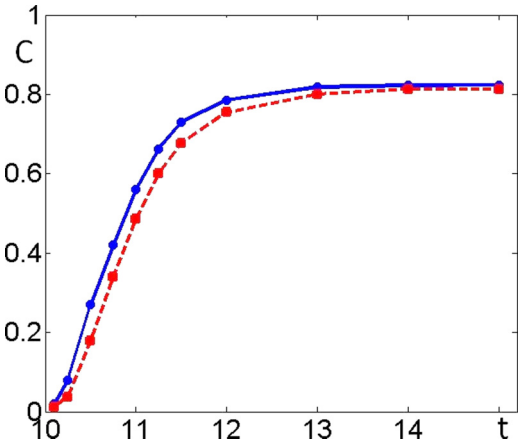

FIG. 13. Phase concentration vs time $p = 5$ and $\gamma = 0.3$ with and without plasticity.

dislocations within the -30° inclined slip system and right grain boundary only, similar to Fig. 6(a) for $p = 1.59$.

2. Concentration of the high-pressure phase

The concentration of HPP c versus time is presented in Fig. 13. The concentration for the case without plasticity is higher than that with plasticity in the right grain during evolution; however, in contrast to that for $p = 1.59$, their difference disappears for larger times, resulting in a similar stationary concentration 0.8 for both cases. Also, after the concentration reaches some initial small value, similar to that for $p = 1.59$, it linearly increases in time until it reaches $c = 0.5$ with plasticity and $c = 0.6$ without plasticity. For larger time, c increases gradually for both cases with plasticity and without it toward the stationary value.

3. Averaged pressure and shear stress

The averaged pressure $\bar{p}$ and shear stress $\bar{\tau}$ are plotted versus time and also concentration in Figs. 14 and 15, respectively. After the concentration reaches some small initial value, both $\bar{p}$ and $\bar{\tau}$ linearly decrease with time until $t = 11$, and then they gradually decrease until they reach the stationary value. The difference between $\bar{p}$ and $\bar{\tau}$ for the cases with and without plasticity is very small for $t < 11.5$, but then, it increases in time. Both $\bar{p}$ and $\bar{\tau}$ almost linearly decrease with HPP concentration for cases both with and without plasticity.

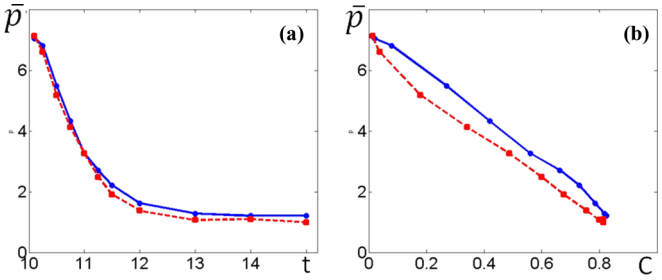

FIG. 14. Average pressure vs time and the high-pressure phase concentration under $p = 5$ and $\gamma = 0.3$ in the right grain with and without plasticity.

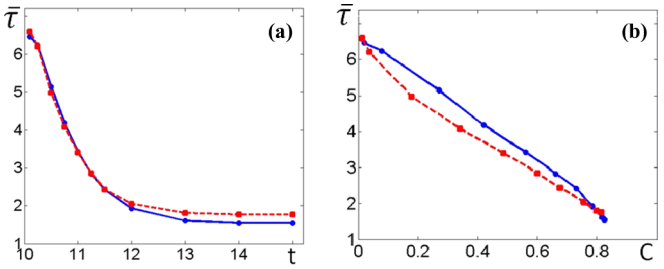

FIG. 15. Average shear vs time and the high-pressure phase concentration under $p = 5$ and $\gamma = 0.3$ in the right grain with and without plasticity.

In contrast to the problem with $p = 1.59$, $\bar{p}$ for the case without plasticity versus time is higher than with plasticity. However, similar to the problem with $p = 1.59$, $\bar{p}$ versus concentration for the case without plasticity is higher than that of the case with plasticity.

In contrast to $\bar{p}$, $\bar{\tau}$ for the case without plasticity is lower than with plasticity for the same time. However, similar to the problem with $p = 1.59$, $\bar{\tau}$ for the case without plasticity is higher than with plasticity for the same concentration. Both $\bar{p}$ and $\bar{\tau}$ versus HPP concentration are almost the same for zero and stationary c for cases with and without plasticity in the right grain, but for intermediate c both stresses with plasticity are lower due to additional stress relaxation.

The stationary pressure is larger for $p = 5$ than for $p = 1.59$ and is compressive. The curve for shear stress versus time and HPP concentration is slightly lower for $p = 5$ than for $p = 1.59$ due to smaller shear.

VI. TRANSFORMATION WORK BASED ANALYSIS

Here, the stationary geometry of the HPP region and HPP concentration will be interpreted utilizing approximate thermodynamic equilibrium conditions across a stationary phase interface and values of the transformation work averaged over the HPP region and the entire transformed grain. The interface energy will be neglected, and transformation work will be evaluated based on small-strain theory. This is done for simplicity, and validity of these assumptions will be justified by obtained results. The local phase equilibrium condition for each interface point of the plastically deformed material in the deformed state, when elastic properties do not change, is based on the transformation work, as it was justified in Refs. [18,19,22,29]:

$$\boldsymbol{\sigma}:\boldsymbol{\varepsilon}_t = \Delta G^{\theta}(\theta) = A_0(\theta - \theta_e)/3. \tag{22}$$

An alternative approach based on utilizing the Eshelby driving force (i.e., total work, including plastic work) [10,23–25] was criticized in Ref. [29]. Distribution of the transformation work $\boldsymbol{\sigma}:\boldsymbol{\varepsilon}_t$ is determined with the help of stress and transformation strain tensor fields. Then, for the chosen temperature $\theta = 298$ K, Eq. (22) defines the contour lines along which the phase equilibrium criterion is met. Also, to check the possibility of description of phase equilibrium conditions in terms of the transformation work averaged over the transformed grain area,

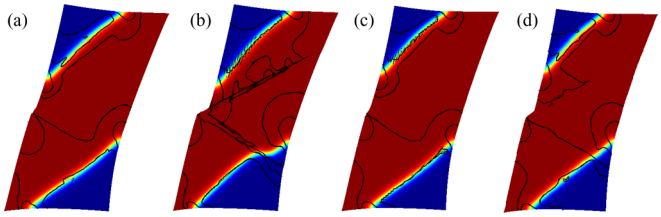

FIG. 16. Stationary phase state and contour lines of the equilibrium transformation work ($\boldsymbol{\sigma}:\boldsymbol{\varepsilon}_t = \Delta^\theta G(\theta) = 0.608$) for case 1 without (a) and with plasticity (b), and for case 2 without (c) and with plasticity (d).

$\langle \dots \rangle_M = \frac{1}{V_M}\int \dots dV_M$, and the total grain area, $\langle \dots \rangle_0 = \frac{1}{V_0}\int \dots dV_0$, we define

$$W_t = \frac{1}{V_0}\int \boldsymbol{\sigma}:\boldsymbol{\varepsilon}_t(\eta) dV_0 \simeq \frac{1}{V_0}\int \boldsymbol{\sigma}:\boldsymbol{\varepsilon}_t dV_M = \langle \boldsymbol{\sigma}:\boldsymbol{\varepsilon}_t\rangle_M c = \langle \boldsymbol{\sigma}\rangle_M:\boldsymbol{\varepsilon}_t c; \quad (23)$$

$$W_t^* = \frac{1}{V_0}\int \boldsymbol{\sigma}:\boldsymbol{\varepsilon}_t dV_0 = \langle \boldsymbol{\sigma}:\boldsymbol{\varepsilon}_t\rangle_0 \simeq \langle \boldsymbol{\sigma}\rangle_0:\boldsymbol{\varepsilon}_t. \quad (24)$$

We used that the phase interface thickness is much smaller than the size of the HPP region (which is true for relatively large c) and that $\boldsymbol{\varepsilon}_t(\eta)$ is homogeneous in the HPP region and equal to zero outside of it. In the definition of W_t^*, we used the same stress distribution and assumed that transformation strain is homogeneous in the entire grain. In contrast to W_t, the definition of W_t^* does not require knowledge of the transformed regions, just resultant stress fields.

The stationary distribution of HPP and contour line of the equilibrium value of PT work are plotted in the right grain for problems with and without plasticity for two different cases: one under $p = 1.59$ and $\gamma = 0.35$ (case 1) and the other under $p = 5$ and $\gamma = 0.3$ (case 2) (Fig. 16). Also, the parameters $\Delta G^\theta(\theta)$, c, W_t, W_t^*, $\langle \boldsymbol{\sigma}\rangle_0:\boldsymbol{\varepsilon}_t$, $\langle \boldsymbol{\sigma}\rangle_M:\boldsymbol{\varepsilon}_t$, the volumetric and deviatoric parts of $\langle \boldsymbol{\sigma}\rangle_0:\boldsymbol{\varepsilon}_t$, as well as the normalized parameters $W_t/\langle \boldsymbol{\sigma}\rangle_M:\boldsymbol{\varepsilon}_t$ and $\langle \boldsymbol{\sigma}\rangle_0:\boldsymbol{\varepsilon}_t/\Delta G^\theta(\theta)$, calculated for the problems without and with plasticity for both cases 1 and 2, are presented in Table I.

TABLE I. Some averaged characteristics of the stationary solutions.

	Without plasticity		With plasticity	
	case 1	case 2	case 1	case 2
c	0.797	0.824	0.762	0.813
$\Delta^\theta G(\theta)$	0.608	0.608	0.608	0.608
$\langle \boldsymbol{\sigma}\rangle_M:\boldsymbol{\varepsilon}_t$	0.665	0.757	0.591	0.723
$\langle \boldsymbol{\sigma}\rangle_0:\boldsymbol{\varepsilon}_t$	0.661	0.733	0.608	0.707
W_t	0.531	0.625	0.451	0.588
W_t^*	0.663	0.731	0.609	0.706
$W_t/\langle \boldsymbol{\sigma}\rangle_M:\boldsymbol{\varepsilon}_t$	0.798	0.826	0.763	0.813
$\langle \boldsymbol{\sigma}\rangle_0:\boldsymbol{\varepsilon}_t/\Delta^\theta G(\theta)$	1.087	1.205	1	1.163
W_t/W_t^*	0.799	0.855	0.741	0.833
$(\langle \boldsymbol{\sigma}\rangle_0:\boldsymbol{\varepsilon}_t)_{\text{vol}}$	−0.286	−0.247	0.202	0.239
$(\langle \boldsymbol{\sigma}\rangle_0:\boldsymbol{\varepsilon}_t)_{\text{dev}}$	0.949	0.856	0.53	0.459

The following noteworthy results are obtained. (a) The concentration of HPP c is approximately equal to the parameter W_t/W_t^*, see Table I for stationary values, Fig. 17 for time evolution, and Fig. 18 for different concentrations c for pressure $p = 1.59$ and the shear $\gamma = 0.35$. The values of these parameters are closer when plasticity in the right grain is neglected.

(b) Consequently, averaged transformation works, $\langle \boldsymbol{\sigma}\rangle_M:\boldsymbol{\varepsilon}_t$ and $\langle \boldsymbol{\sigma}\rangle_0:\boldsymbol{\varepsilon}_t$, are quite close as well. This means approximate equality of the two averaged stress tensors, $\langle \boldsymbol{\sigma}\rangle_M \simeq \langle \boldsymbol{\sigma}\rangle_0$. This is surprising because of the very heterogeneous stress field, but it is in agreement with the results obtained for the shear-induced PT without pressure [8].

(c) As can be seen from Fig. 16, the contour lines corresponding to $\boldsymbol{\sigma}:\boldsymbol{\varepsilon}_t = \Delta^\theta G(\theta)$ are close to the phase interfaces almost everywhere, both with and without plasticity. This was quite an unexpected result taking into account the strong heterogeneity of all fields, significant internal stresses, and strong stress concentrators. All deviations are near the intersections of the phase interface with the grain boundaries and phase interfaces coinciding with the grain boundaries, which creates an additional driving force for moving the triple junctions.

(d) While generally $\langle \boldsymbol{\sigma}\rangle_0:\boldsymbol{\varepsilon}_t$ is not equal to $\Delta^\theta G(\theta)$, the difference is within 9% for case 1 and within 20% for case 2. The perfect coincidence is for case 1 with plasticity in the transforming grain. Transformation work $\langle \boldsymbol{\sigma}\rangle_M:\boldsymbol{\varepsilon}_t$ has a larger deviation from $\Delta^\theta G(\theta)$ than $\langle \boldsymbol{\sigma}\rangle_0:\boldsymbol{\varepsilon}_t$. This approximate equality will allow us to develop in future approximate methods of nano- to microscale coarse graining approach and microscale averaged description of strain-induced PTs in terms of microscale phase equilibrium criterion $\langle \boldsymbol{\sigma}\rangle_0:\boldsymbol{\varepsilon}_t \simeq \Delta^\theta G(\theta)$ and concentration c. Current microscale description [6,93,115] do not include detailed nano- to macroscale transition and can definitely benefit from the current results. Note that the difference between $\langle \boldsymbol{\sigma}\rangle_0:\boldsymbol{\varepsilon}_t$ and $\Delta^\theta G(\theta)$ increases with pressure and was very small for zero pressure in Ref. [8].

(e) Stationary phase interfaces contain no dislocations or only a single dislocation, despite large plastic deformation in the transforming grain. This, however, corresponds to some experiments [101,102] where the major part of the interfaces was dislocation-free (i.e., coherent) after large plastic deformations utilizing high-pressure torsion.

(f) Decomposing transformation work $\langle \boldsymbol{\sigma}\rangle_0:\boldsymbol{\varepsilon}_t = -\langle p\rangle_0\varepsilon_{0t} + \langle \boldsymbol{S}\rangle_0:\boldsymbol{e}_t$ into work of pressure and deviatoric stress $\langle \boldsymbol{S}\rangle_0$, where $\varepsilon_{0t} = -0.1$ and $\boldsymbol{e}_t$ is the volumetric and deviatoric parts of the transformation strain, we can analyze their relative contributions (Table I). In all cases, the contribution of the deviatoric transformation work is significantly larger than the work of pressure. In fact, for $p = 1.59$ without plasticity in the transforming grain, the contribution of pressure is even negative due to its drop to negative values caused by volumetric transformation strain (Fig. 9). Thus, in contrast to earlier statements in Refs. [6,93], where contribution of applied shear stresses to the transformation work was negligible, for the given PT and nanograined material, the effect of the averaged shear stresses is the major one. This is because of relatively low applied pressure, a large transformed region and corresponding local pressure drop, and higher yield strength due to grain size effect and relatively high-yield strength of the HPP.

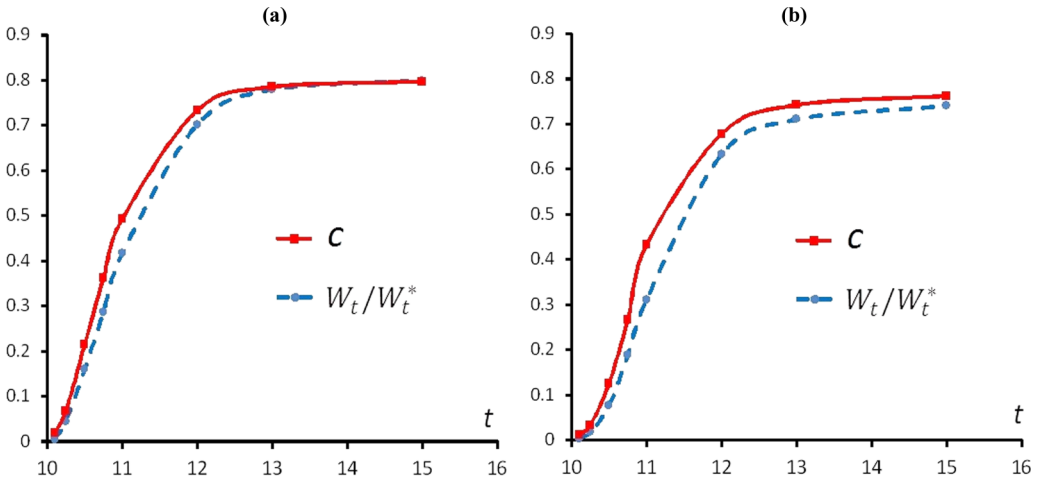

FIG. 17. Comparison of the time dependence of the HPP concentration c and the ratio W_t/W_t^* in the right grain without plasticity (a) and with plasticity (b) under the pressure $p = 1.59$ and the shear $\gamma = 0.35$.

The transformation work W_t versus time and concentration is presented in Fig. 19 for $p = 1.59$ and in Fig. 20 for $p = 5$, for both cases with and without plasticity in the right grain. As can be seen, for $p = 1.59$, W_t increases almost linearly in time until $t = 11$ when it reaches the concentration $c = 0.49$ without plasticity and $c = 0.4$ with plasticity. Then, it grows slower until it reaches its maximum value at $t = 11.25$ with $W_t = 0.7$ without plasticity and $W_t = 0.6$ with plasticity, at the same concentration $c \simeq 0.6$. In the following, transformation work gradually decreases until it reaches the stationary value $W_t = 0.52$ without plasticity and $W_t = 0.45$ with plasticity. The transformation work W_t also initially increases with concentration for both cases, with a reduced rate, until it reaches its maximum value at $c \simeq 0.6$ and decreases toward its stationary solution. It is evident that plasticity in the transforming grain reduces transformation work due to stress relaxation. The difference between values W_t for cases without and with plasticity increases until it reaches maximum at $t = 11.25$, and then it becomes almost constant until the stationary solutions are reached. The same plots in Fig. 20 for $p = 5$ are qualitatively similar but with slightly larger maximum and stationary values of transformation work. Interestingly, the maximum of W_t is reached at the same time and HPP concentration as for both applied pressures.

The transformation work W_t^* is plotted versus time in Fig. 21 for $p = 1.59$ and $\gamma = 0.35$ (a) and for $p = 5$ and $\gamma = 0.3$ (b) based on results for average stresses in Figs. 9, 10, 14, and 15. As can be seen, the plot W_t^* vs time repeats the character of plots for averaged pressure and shear stress vs time, i.e., it has a maximum at the beginning when the stress concentration due to dislocation pile-up and applied stresses did not start relaxing, and reduces in time due to stress relaxation due to PT and dislocations. The transformation work W_t^* is very close for both cases with and without plasticity in the right grain. Thus the difference between W_t for both cases is proportional to the difference between the corresponding HPP concentrations at the same time. As shown in Fig. 8, the difference between the concentrations with and without plasticity initially increases until the maximum transformation work is reached then decreases and becomes constant; the same is observed for W_t versus time (Fig. 19).

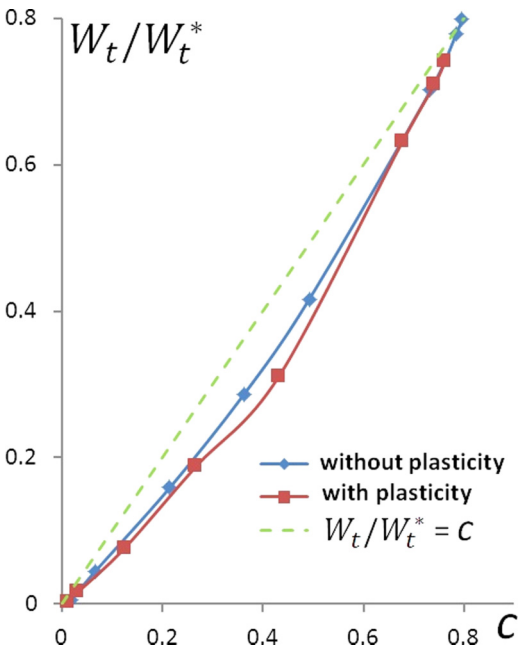

FIG. 18. The ratio W_t/W_t^* vs the HPP concentration c in the right grain with and without plasticity under the pressure $p = 1.59$ and the shear $\gamma = 0.35$. The line $W_t/W_t^* = c$ is plotted for comparison.

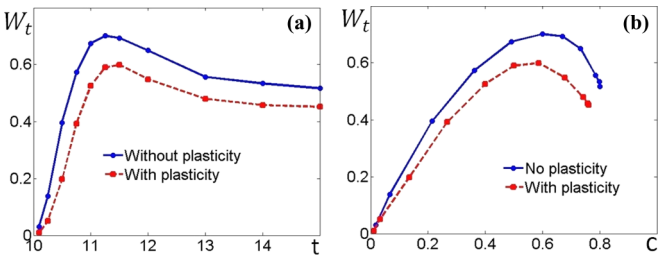

FIG. 19. Transformation work vs time and the high-pressure phase concentration under $p = 1.59$ and $\gamma = 0.35$ in the right grain with and without plasticity.

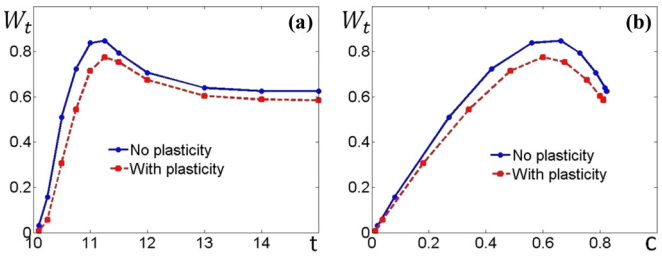

FIG. 20. Transformation work vs time and the high-pressure phase concentration under $p = 5$ and $\gamma = 0.3$ in the right grain with and without plasticity in the right grain.

VII. MINIMUM SHEAR AND NUMBER OF DISLOCATIONS IN A PILE-UP FOR HPP NUCLEATION

As it was shown above, the least number of dislocations in a pile-up in the left grain required to nucleate HPP in the presence of $\pm 30^\circ$ inclined dislocations in the right grain, and the corresponding applied shear, were found for three pressures, 0, 1.59, and 5. Also, under the hydrostatic conditions, we accepted one dislocation per two nanograins and obtained $p_h = 15.9$ for HPP nucleation. The required number of dislocations in the left grain for HPP nucleation and the corresponding applied shear are plotted versus the applied normal stress in Figs. 22 and 23, respectively. The number of dislocations required for HPP nucleation linearly decreases with increasing pressure, which is in agreement with our analytical estimates in Refs. [6,93]. However, the required shear first surprisingly increases when pressure increases from 0 to 1.59, and then it linearly decreases, as expected. Note that if for $p = 1.59$, we take into account that at $\gamma = 0.3$ HPP, nucleation does occur in the right grain (while not at the tip of dislocation pile-up located in the left grain, see Sec. V C), we obtain that critical shear strain for HPP of 0.3 is the same in the pressure range from 0 till 5. Due to complex interaction between plasticity in both grains and PT, it is difficult to give a simple interpretation of this nonmonotonous dependence or independence of the critical shear for HPP nucleation on pressure. Note that the stationary concentration of HPP, after fulfilling the nucleation condition, increases with increasing pressure in the pressure range from 0 till 5.

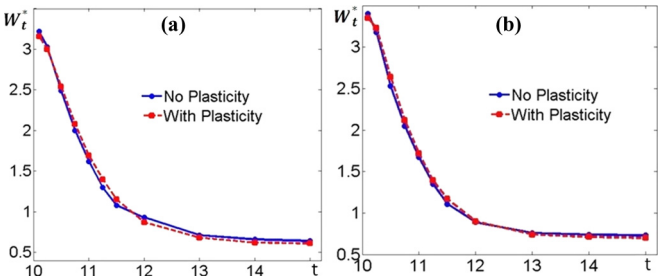

FIG. 21. W_t^* vs time for $p = 1.59$ and $\gamma = 0.35$ (a) and for $p = 5$ and $\gamma = 0.3$ (b) in the right grain with and without plasticity.

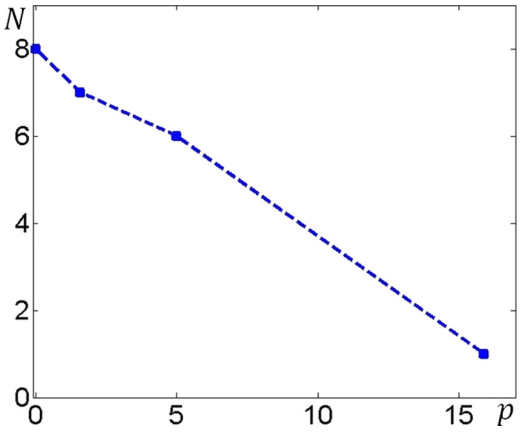

FIG. 22. The least number of dislocations piled up in the left grain vs the applied pressure to nucleate HPP in the right grain.

VIII. THE EFFECT OF THE RATIO OF KINETIC COEFFICIENTS FOR PHASE TRANSFORMATION AND DISLOCATION EVOLUTION ON THE NANOSTRUCTURE EVOLUTION

It is qualitatively clear that the ratio of kinetic coefficients for PT and dislocations L_η/L_ξ determine the relative rate of these two competing processes and consequently affects the nanostructure evolution. However, does L_η/L_ξ affect the stationary solution and nanostructure? An *a priori* guess would be it does not, because stationary Ginzburg-Landau equations for PT and dislocations do not even include L_η and L_ξ. To elucidate this effect, the same interaction problem at $p = 5$ and $\gamma = 0.3$ and the same PT kinetics coefficient but with different

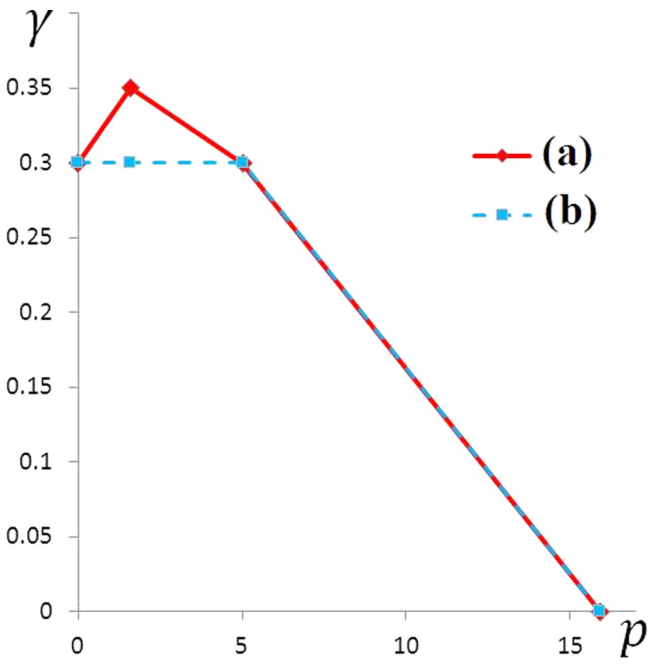

FIG. 23. The minimum applied shear strain vs the applied pressure to nucleate HPP in the right grain: (a) HPP nucleation only at the tip of dislocation pile-up located in the left grain and (b) HPP nucleation at any place in the right grain.

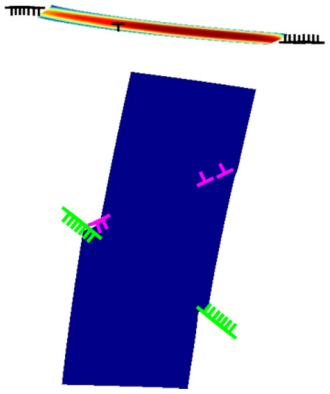

FIG. 24. The phase and dislocations solution at $t = 0.75$ under $p = 5$ and $\gamma = 0.3$ with five times larger $L_\xi = 5 \times 10^4$ $(\text{Pa s})^{-1}$ ($L_\eta/L_\xi = 0.052$). High-pressure phase does not nucleate.

kinetics coefficients for dislocations are solved. In addition to solutions in Fig. 11 with $L_\eta/L_\xi = 2600/10000 = 0.26$, we considered 5 times larger kinetics coefficient for dislocations, i.e., $L_\eta/L_\xi = 0.052$, and another one with the same kinetics coefficients for both PTs and dislocations, $L_\eta/L_\xi = 1$. For the smaller ratio $L_\eta/L_\xi = 0.052$, in contrast to the previous solution with $L_\eta/L_\xi = 0.26$ (Fig. 11), HPP does not nucleate, and only dislocations are generated and evolve. Figure 24 shows the corresponding nanostructure at $t = 0.75$. As can be seen, the number of dislocations is larger than that in the problem with a lower kinetics coefficient, stresses in the right grain relax much faster by dislocation generation, and they are not sufficient to nucleate the HPP. For the larger $L_\eta/L_\xi = 1$ (Fig. 25), growth of HPP is faster in comparison to that at $L_\eta/L_\xi = 0.26$ (Fig. 11) resulting in a larger concentration c and a smaller number of dislocations. For example, the stationary solution for $L_\eta/L_\xi = 0.26$ contains nine dislocations in the left grain, four dislocations in the $+30^\circ$ inclined slip plane, and two dislocations in the -30° inclined slip plane in the right side, while for $L_\eta/L_\xi = 1$, it contains seven dislocations in the left grain, four dislocations in the $+30^\circ$ inclined slip plane, and 1 dislocation in the -30° inclined slip plane in the right side. Also, no HPP appears near the tip of the -30° inclined slip plane at its right end because a -30° inclined dislocation cannot reach the right end due to the smaller kinetic coefficient and cannot create any stress concentration before it reaches the stationary solution.

Thus an increase in the ratio L_η/L_ξ, first allows HPP to nucleate and, second, it allows PT to take over dislocations in the stress relaxation process, reducing the number of dislocations and increasing the HPP zone. Surprisingly, in contrast to our natural guess, the stationary solution does depend on L_η/L_ξ. That means that there are multiple stationary solutions for the same p, γ and transformation and plastic deformation processes are path-dependent.

IX. LACK OF THE SAMPLE SIZE EFFECT IN THE INTERACTION BETWEEN PHASE TRANSFORMATION AND DISLOCATIONS

To study the effect of the sample size, we considered the same sample with two times larger sizes, i.e., 120×120, and with all subdomains proportionally enlarged. To be able to compare with an analytical solution [6,93] for nucleation of HPP at the tip of dislocation pile-up in an infinite space, we solved the same problem as above for only PT (no plasticity inside the right grain) under pressure 1.59 and two different values of shear, $\gamma = 0.2$ and $\gamma = 0.35$. Figure 26 presents the corresponding stationary solutions for both sizes and two different applied shears. As can be seen, for $\gamma = 0.2$, the number of dislocations for the smaller and larger samples reach six and eight, respectively. In the analytical solution [6,93], local stresses at the tip of the dislocation pile-up are proportional to the number of dislocations, and we observed the same in our simulations. However, the average pressure and shear stress, and the concentration of HPP are very close for both sizes. For the smaller size, $\bar{p} = 3.16$ and $\bar{\tau} = 4.53$ before HPP nucleation, and $\bar{p} = -0.01$, $\bar{\tau} = 1.93$, and $c = 0.48$ for

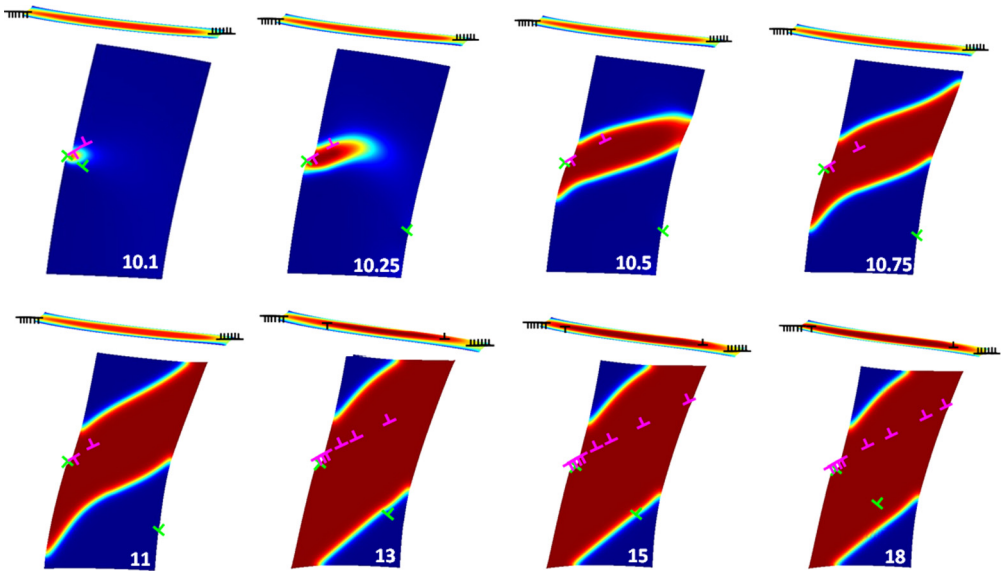

FIG. 25. Evolution of the dislocations under $p = 5$ and $\gamma = 0.3$ with plasticity in the right grain for smaller $L_\xi = 2600$ ($L_\eta/L_\xi = 1$).

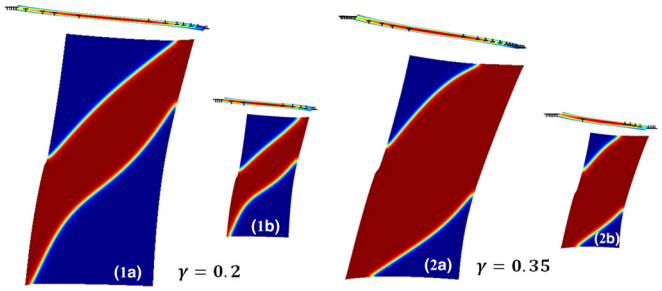

FIG. 26. Stationary solutions for two different sample sizes of 120×120 (a) and 60×60 (b), and two different applied shears $\gamma = 0.2$ (1) and $\gamma = 0.35$ (2).

the stationary solution. For the larger size, $\bar{p} = 3.22$ and $\bar{\tau} = 4.48$ before HPP nucleation, and $\bar{p} = -0.07$, $\bar{\tau} = 1.89$, and $c = 0.47$ for the stationary solution. Thus the larger grain size results in more dislocations and, consequently, higher stress concentration, but due to the larger area of the transforming grain and larger distance from the tip of dislocation pile-up, the results do not change. The same is observed for $\gamma = 0.35$. Here, the number of dislocations for the smaller and larger samples reached 9 and 14, respectively. For the smaller size, $\bar{p} = 4.46$ and $\bar{\tau} = 7.84$ before HPP nucleation, and $\bar{p} = -1.43$, $\bar{\tau} = 3.16$, and $c = 0.80$ for the stationary solution. For the larger size, $\bar{p} = 4.52$ and $\bar{\tau} = 7.86$ before HPP nucleation, and $\bar{p} = -1.3$, $\bar{\tau} = 3.2$, and $c = 0.79$ for the stationary solution. Thus obtained results are independent of the size of the sample.

Let us compare some results with an analytical solution [6,93]. One of the points of solution for stresses is that at fixed applied (averaged) shear stress $\bar{\tau}$, the ratio N/l of the number of piled up dislocations to the dislocation pile-up length is constant. Since N changes with the sample size, the length of the pile-up should change proportionally, i.e., $N^l/N^s = l^l/l^s$, where superscripts s and l stand for smaller and larger sizes, respectively. For $\gamma = 0.35$, $l^s = 13.2$ (determined in the undeformed configuration), $N^s = 9$, $l^l = 17.6$, and $N^l = 13$. Thus $l^l/l^s = 1.3$ and $N^l/N^s = 1.4$, which are quite close. However, for $\gamma = 0.2$, we obtained $l^s = 8.2$, $N^s = 6$, $l^l = 18.2$, and $N^l = 8$, which gives $l^l/l^s = 2.2$ and $N^l/N^s = 1.3$. These results do not correspond to analytical predictions for an infinite space.

Also, according to the analytical solution, the combination $N/(l\bar{\tau})$ should be a constant independent of the applied shear stress $\bar{\tau}$. In our simulations, for $\gamma = 0.35$, $N^s/(l^s\bar{\tau}^s) \simeq 0.19$ and $N^l/(l^l\bar{\tau}^l) = 0.2$, which is close, but for $\gamma = 0.2$ one has $N^s/(l^s\bar{\tau}^s) \simeq 0.36$, $\mathrm{N}^l/(l^l\bar{\tau}^l) = 0.21$, which is not.

In addition, in analytical solution [6,93], the same transformation pressure for the same applied shear stress $\bar{\tau}$ is obtained when the ratio l/R is constant, where R is the largest size of the box-shape HPP nucleus with large aspect ratio. In our simulations, due to finite grain size, the largest size of nucleus is fully determined by the grain size, and stationary nucleus geometry is not determined by the dislocation pile-up (like in Ref. [6,93]), but by a constraint imposed by the grain size and shape. One may assume that the same transformation pressure for the same applied shear stress $\bar{\tau}$ should correspond to the same ratio l as the grain or sample size. However, while sample size changed by a factor of 2, $l^l/l^s = 1.57$, i.e., there is no geometric similarity. This means that due to significant difference between problem formulation in Refs. [6,93] and here, not all quantitative conclusions can be transferred. Nevertheless, our results show the lack of the sample-size effect on the averaged stresses, concentration of HPP and geometry of the HPP, which is unexpected and therefore quite valuable.

X. CONCLUDING REMARKS

In the paper, the general PFA for the interaction between PT and dislocation evolution developed in Ref. [62] is applied for FEM simulations of the pressure and shear strain-induced phase transformation coupled with plasticity in a bicrystal at the evolving dislocations pile-up in the left grain. The slip system of the LPP (or HPP) transformed during a PT to HPP (or LPP) coincide with slip systems of HPP (or LPP). The lowest pressure at which HPP nucleus appears under hydrostatic conditions was determined to be 15.9 GPa. To study the pressure and shear-induced PTs, three different pressures (0, 1.59, and 5 GPa) were considered. Due to applied shear, dislocations nucleate in the left grain, after which they pile-up near grain boundaries and produce a strong stress tensor concentrator, which leads to the increase in the local thermodynamic driving force for PT in the region near the dislocation pile-up tip and causes barrierless HPP nucleation in the right grain. Surprisingly, a HPP nucleus appears even at zero pressure. At pressures of 1.59 and 5 GPa and shear, a major part of a grain transforms to HPP. This *conceptually proves that the dislocation pile-up mechanism is able to reduce PT pressure due to applied shear by an order of magnitude*, as it was observed in experiments [6,93,96,114]. When dislocations in the right grain are included, they relax stress concentration, which reduces stresses, the driving force for PT and, consequently, HPP concentration. Plasticity in the right grain not only slightly suppresses PT but also increases the number of dislocations in the pile-up in the left grain. Generally, the effect of plasticity in the transforming grain on the growth stage and stationary solution under current boundary conditions at the lateral surface (applied normal stress) is less pronounced than for periodic boundary conditions in Ref. [64]. However, plasticity in the transforming grain strongly increases the number of dislocations in the pile-up required for nucleation of the HPP and corresponding shear.

For each applied pressure, the least number of dislocations and corresponding applied shear required to cause nucleation were found. The least number of dislocations in a pile-up to nucleate HPP linearly decreases with increasing applied pressure. However, the minimum applied shear to nucleate HPP changes nonmonotonously with increased applied pressure. The final stationary HPP morphology and concentration for cases both with and without plasticity in the transforming grain are found to be governed by the simplest local thermodynamic equilibrium at the interfaces, i.e., by local transformation work [see Eq. (22)]. Plastic work does not contribute to the phase equilibrium, which corroborates macroscale approaches in Refs. [9,18,19,22,26–29] and contradicts the approach based on the Eshelby driving force [10,24]. Also, the stationary

nanostructure can be approximately described by the thermodynamic equilibrium conditions in terms of stresses averaged over the HPP region or the entire grain. This means, in particular, equality of the transformation work at the points of phase interface and in terms of averaged stresses over the HPP and over the entire grain, which is very nontrivial considering the high-stress concentration and heterogeneity.

These results are very unexpected also because we neglected interface energy and athermal interface friction. They give exactly the opposite picture in comparison with the previous studies [6,93], where it was stated that phase equilibrium conditions do not enter the macroscopic (averaged) description of strain-induced PTs. The reason is the consideration of a much smaller scale here than in the microscale and macroscale treatments in Refs. [6,93].

In particular, we found that, in a stationary state, the major part of the interface is dislocation-free (i.e., coherent), which is in accordance with some experiments [101,102]. Since here dislocations near the interface provide the only source of the athermal interface friction, this explains lack of the athermal friction in the obtained phase equilibrium conditions.

It was also found that the contribution of the deviatoric transformation work is significantly larger than the work of pressure. In fact, for $p = 1.59$, an averaged pressure and its contribution to the transformation work are even negative due to compressive volumetric transformation strain. This is in contrast to earlier statements in Refs. [6,93], where the contribution of applied shear stresses to the transformation work was negligible. This is caused by a relatively low applied pressure and higher yield strength due to grain size effect and due to stronger HPP than the LPP.

Also, in the nanograin material, the region with a strong stress concentrator is comparable with the entire grain, which leads to a large transformed region, relaxing stress concentration. With allowed plasticity in the transformed grain, stresses further relax and become more homogeneous.

Surprisingly, the ratio of kinetic coefficients for PT and dislocations affects the stationary solution and nanostructure despite the fact that they do not explicitly participate in the formulation of the stationary problem. Consequently, there are multiple stationary solutions under the same applied load and PT, and deformation processes are path dependent. The faster the dislocations are in comparison with PT, the larger number of dislocations appears and stress relaxation causes reduction in the HPP region. In particular, at $p = 5$ and $\gamma = 0.3$ with 5 times larger $L_\xi = 5 \times 10^4\,(\mathrm{Pa\,s})^{-1}$ ($L_\eta/L_\xi = 0.052$), the HPP does not nucleate. By increasing the size of the sample by a factor of two, no effect was found on the averaged pressure and shear stress and HPP nanostructure, despite the larger number of dislocations in a pile-up for a larger sample and, consequently, larger local stresses.

Obtained results represent a nanoscale basis for understanding and description of PTs under compression and shear in rotational diamond anvil cell and high-pressure torsion. It will be used for developing microscale kinetics as a result of a nano- to microtransition. Since the main results of the current nanoscale treatment are quite different from those in Refs. [6,64,93], microscale equations will be different as well. New microscale equations will substitute the current model in the macroscale studies of the behavior of a sample in RDAC, see Refs. [114–119]. Also, a similar approach for the interaction between PT and plasticity is important and can be applied for studying friction, indentation, surface treatment, ball milling, and projectile penetration.

It is clear that some quantitative results obtained here (e.g., evolution of concentration of the HPP) will be changed when a more precise 3D formulation is used. However, we believe the following main important qualitative findings will remain the same: (a) fulfillment of the simplest local thermodynamic equilibrium condition, Eq. (22), for most of the points of the interface; (b) approximate fulfillment of the same thermodynamic equilibrium condition with the stresses averaged over the transformed region or the entire grain and the possibility of utilizing these criterion for coarse graining at the microscale; (c) prevailing the deviatoric contribution to the transformation work over the contribution due to the hydrostatic pressure; (d) a possibility of reducing the transformation pressure by an order of magnitude and in some cases down to zero; (e) the presence of multiple stationary dislocation and phase structures under the same conditions that depend on the ratio of the kinetic coefficients for dislocation evolution and PTs; (f) lack of the scale effect for the interaction between PTs and plasticity. Five of the six results were not reported in Ref. [64], and the sixth one was reported partially (without zero pressure).

ACKNOWLEDGMENTS

This work was supported by NSF (CMMI-1536925 and DMR-1434613), ARO (W911NF-12-1-0340), ONR (N00014-16-1-2079), Iowa State University (Schafer 2050 Challenge Professorship), and Isfahan University of Technology.

[1] G. B. Olson, Science **277**, 1237 (1997).
[2] G. B. Olson and M. Cohen, in *Dislocations in Solids*, edited by F. R. N. Nabarro (North-Holland, Amsterdam, 1986), Vol. 7, p. 297.
[3] F. D. Fischer, M. Berveiller, K. Tanaka, and E. Oberaigner, Arch. Appl. Mech. **64**, 54 (1994).
[4] G. B. Olson and A. L. Roytburd, in *Martensite*, edited by G. B. Olson and W. S. Owen (The Materials Information Society, Novelty, OH, 1995), Vol. 9, p. 149.
[5] F. D. Fischer, Q.-P. Sun, and K. Tanaka, Appl. Mech. Rev. **49**, 317 (1996).
[6] V. I. Levitas, in *Continuum Mechanical Fundamentals of Mechanochemistry*, edited by Y. Gogotsi and V. Domnich, High Pressure Surface Science and Engineering. Section 3 (Institute of Physics Publishing, London, UK, 2004), p. 159.
[7] F. C. Lovey and V. Torra, Prog. Mater. Sci. **44**, 189 (1999).
[8] M. Javanbakht and V. I. Levitas, J. Mech. Phys. Solids **82**, 164 (2015).

[9] V. I. Levitas, A. V. Idesman, G. B. Olson, and E. Stein, Philos. Mag. A **82**, 429 (2002).
[10] F. D. Fischer *et al.*, Int. J. Plast. **16**, 723 (2000).
[11] A. L. Roitburd and D. E. Temkin, Sov. Phys. Solid State **28**, 432 (1986).
[12] I. M. Kaganova and A. L. Roitburd, Sov. Phys. Solid State **31**, 545 (1989).
[13] F. Marketz and F. D. Fischer, Comput. Mater. Sci. **3**, 307 (1994).
[14] F. Marketz and F. D. Fischer, Mater. Trans. A **26**, 267 (1995).
[15] V. I. Levitas, J. de Physique IV **5**, 173 (1995).
[16] V. I. Levitas, J. de Physique IV **5**, 41 (1995).
[17] V. I. Levitas, J. de Physique IV **6**, 55 (1996).
[18] V. I. Levitas, J. Mech. Phys. Solids. **45**, 923 (1997); **45**, 1203 (1997).
[19] V. I. Levitas, Int. J. Solids Struct. **35**, 889 (1998).
[20] V. I. Levitas, Int. J. Eng. Sci. **33**, 921 (1995).
[21] V. I. Levitas, Int. J. Eng. Sci. **33**, 947 (1995).
[22] V. I. Levitas, Int. J. Plast. **16**, 805 (2000); **16**, 851 (2000).
[23] M. Cherkaoui, M. Berveiller, and H. Sabar, Int. J. Plast. **14**, 597 (1998).
[24] M. Cherkaoui and M. Berveiller, Arch. Appl. Mech. **70**, 159 (2000).
[25] F. D. Fischer and G. Reisner, Acta Mater. **46**, 2095 (1998).
[26] A. V. Idesman, V. I. Levitas, and E. Stein, Int. J. Solids Struct. **35**, 855 (1998).
[27] A. V. Idesman, V. I. Levitas, and E. Stein, Comp. Meth. Appl. Mech. Eng. **173**, 71 (1999).
[28] A. V. Idesman, V. I. Levitas, and E. Stein, Int. J. Plast. **16**, 893 (2000).
[29] V. I. Levitas, Int. J. Plast. **18**, 1499 (2002).
[30] V. I. Levitas, A. V. Idesman, and G. B. Olson, Acta. Mater. **47**, 219 (1999).
[31] J. Shi, S. Turteltaub, and E. Van der Giessen, J. Mech. Phys. Solids. **58**, 1863 (2010).
[32] V. I. Levitas, Int. J. Plast. **49**, 85 (2013).
[33] V. I. Levitas and D. L. Preston, Phys. Rev. B **66**, 134206 (2002).
[34] V. I. Levitas and D. L. Preston, Phys. Rev. B **66**, 134207 (2002).
[35] V. I. Levitas, D. L. Preston, and D. W. Lee, Phys. Rev. B **68**, 134201 (2003).
[36] Y. M. Jin, A. Artemev, and A. G. Khachaturyan, Acta. Mat. **49**, 2309 (2001).
[37] Y. Wang and A. G. Khachaturyan, Acta. Mater. **45**, 759 (1997).
[38] A. Artemev, Y. Jin, and A. G. Khachaturyan, Acta. Mater. **49**, 1165 (2001).
[39] L. Q. Chen, Annu. Rev. Mater. Res. **32**, 113 (2002).
[40] V. I. Levitas, V. A. Levin, K. M. Zingerman, and E. I. Freiman, Phys. Rev. Lett. **103**, 025702 (2009).
[41] V. I. Levitas and D. W. Lee, Phys. Rev. Lett. **99**, 245701 (2007).
[42] V. I. Levitas, D. W. Lee, and D. L. Preston, Int. J. Plast. **26**, 395 (2010).
[43] A. V. Idesman, J. Y. Cho, and V. I. Levitas, Appl. Phys. Lett. **93**, 043102 (2008).
[44] J. Y. Cho, A. V. Idesman, V. I. Levitas, and T. Park, Int. J. Solids Struct. **49**, 1973 (2012).
[45] V. A. Levin, V. I. Levitas, K. M. Zingerman, and E. I. Freiman, Int. J. Solids Struct. **50**, 2914 (2013).
[46] Y. U. Wang, Y. M. Jin, A. M. Cuitino, and A. G. Khachaturyan, Acta Mater. **49**, 1847 (2001).
[47] Y. U. Wang and J. Li, Acta. Mater. **58**, 1212 (2010).
[48] S. Y. Hu and L. Q. Chen, Acta. Mater. **49**, 463 (2010).
[49] S. Y. Hu and L. Q. Chen, Comput. Mater. Sci. **23**, 270 (2002).
[50] Y. M. Jin and A. G. Khachaturyan, Phil. Mag. Lett. **81**, 607 (2001).
[51] M. Koslowski, A. M. Cuitino, and M. Ortiz, J. Mech. Phys. Solids **50**, 2597 (2002).
[52] S. Y. Hu, Y. L. Li, Y. X. Zheng, and L. Q. Chen, Int. J. Plast. **20**, 403 (2004).
[53] A. Hunter, I. J. Beyerlein, T. C. Germann, and M. Koslowski, Phys. Rev. B **84**, 144108 (2011).
[54] F. R. N. Nabarro, Phil. Mag. **42**, 1224 (1951).
[55] R. Peierls, Proc. Phys. Soc. London **52**, 34 (1940).
[56] F. R. N. Nabarro, Proc. Phys. Soc. London **59**, 256 (1947).
[57] J. P. Hirth and J. Lothe, *Theory of Dislocations* (Krieger, Malabar, Florida, 1992).
[58] T. Mura, *Micromechanics of Defects in Solids* (Martinus Nijhof, Hague, 1982).
[59] V. I. Levitas and M. Javanbakht, Phys. Rev. B **86**, 140101(R) (2012).
[60] V. I. Levitas and M. Javanbakht, J. Mech. Phys. Solids **82**, 345 (2015).
[61] M. Javanbakht and V. I. Levitas, Int. J. Solids Struct. **82**, 15 (2016).
[62] V. I. Levitas and M. Javanbakht, J. Mech. Phys. Solids **82**, 287 (2015).
[63] V. I. Levitas and M. Javanbakht, Appl. Phys. Lett. **102**, 251904 (2013).
[64] V. I. Levitas and M. Javanbakht, Nanoscale **6**, 162 (2014).
[65] A. L. Korzhenevskii, R. Bausch, and R. Schmitz, Phys. Rev. Lett. **91**, 236101 (2003).
[66] A. C. E. Reid, G. B. Olson, and B. Moran, Phase Trans. **69**, 309 (1998).
[67] Y. Wang and A. G. Khachaturyan, Mater. Sci. Eng. A **438-440**, 55 (2006).
[68] J. Kundin, H. Emmerich, and J. Zimmer, Philos. Mag. **91**, 97 (2011).
[69] A. R. Oganov *et al.*, Nature (London) **457**, 863 (2009).
[70] Y. L. Li *et al.*, Nat. Commun. **6**, 6974 (2015).
[71] M. I. Eremets *et al.*, Nat. Mater. **3**, 558 (2004).
[72] A. Sengupta, M. Kim, C.-S. Yoo, and J. S. Tse, J. Phys. Chem. C **116**, 2061 (2012).
[73] L. Wang *et al.*, Science **337**, 825 (2012).
[74] W. L. Mao *et al.*, Science **302**, 425 (2003).
[75] V. L. Solozhenko, O. O. Kurakevych, D. Andrault, Y. LeGodec, and M. Mezouar, Phys. Rev. Lett. **102**, 015506 (2009).
[76] V. L. Solozhenko and O. O. Kurakevych, J. Solid State Chem. **182**, 1359 (2009).
[77] V. L. Solozhenko *et al.*, Appl. Phys. Lett. **78**, 1385 (2001).
[78] Y. Zhao *et al.*, J. Mater. Res. **17**, 3139 (2002).
[79] R. Zhou and X-C. Zeng, J. Am. Chem. Soc. **134**, 7530 (2012).
[80] C. S. Xu, B. Xu, Y. Yang, H. Dong, A. R. Oganov, S. Wang, W. Duan, B. Gu, and L. Bellaiche, Phys. Rev. B **91**, 020101(R) (2015).
[81] C-S. Zha, Z. Liu, and R. J. Hemley, Phys. Rev. Lett. **108**, 146402 (2012).
[82] H. Xiao *et al.*, Proc. Natl. Acad. Sci. USA **110**, 5321 (2013).
[83] X. Y. Meng *et al.*, Chem Mater. **28**, 1335 (2016).
[84] P. W. Bridgman, Phys. Rev. **48**, 825 (1935).
[85] M. M. Alexandrova, V. D. Blank, and S. G. Buga, Solid State Phys. **35**, 1308 (1993).
[86] M. I. Eremets *et al.*, J. Chem. Phys. **120**, 10618 (2004).

[87] M. Popov, Phys. Lett. A **334**, 317 (2005).
[88] V. I. Levitas, Y. Ma, E. Selvi, J. Wu, and J. A. Patten, Phys. Rev. B **85**, 054114 (2012).
[89] V. D. Blank *et al.*, Phys. Lett. A **188**, 281 (1994).
[90] N. V. Novikov, S. B. Polotnyak, L. K. Shvedov, and V. I. Levitas, J. Superhard Mater. **3**, 36 (1999).
[91] V. I. Levitas and L. K. Shvedov, Phys. Rev. B **65**, 104109 (2002).
[92] M. Popov, M. Kyotania, and Y. Kogaa, Diam. Relat. Mater. **12**, 833 (2003).
[93] V. I. Levitas, Phys. Rev. B **70**, 184118 (2004).
[94] V. I. Levitas, Y. Ma, J. Hashemi, M. Holtz, and N. Guven, J. Chem. Phys. **125**, 044507 (2006).
[95] C. Ji, V. I. Levitas, H. Zhu, J. Chaudhuri, A. Marathe, and Y. Ma, Proc. Natl. Acad. Sci. USA **109**, 19108 (2012).
[96] V. D. Blank and E. I. Estrin, *Phase Transitions in Solids under High Pressure* (CRC Press, Boca Raton, 2014).
[97] M. T. Perez-Prado and A. P. Zhilyaev, Phys. Rev. Lett. **102**, 175504 (2009).
[98] A. P. Zhilyaev *et al.*, Mater. Sci. Eng. A **528**, 3496 (2011).
[99] B. Srinivasarao, A. P. Zhilyaev, and M. T. Perez-Prado, Scripta Mater. **65**, 241 (2011).
[100] R. Z. Valiev, R. K. Islamgaliev, and I. V. Alexandrov, Prog. Mater. Sci. **45**, 103 (2000).
[101] A. P. Zhilyaev and T. G. Langdon, J. Mater. Sci. **47**, 7888 (2012).
[102] K. Edalati, S. Toh, Y. Ikom, and Z. Horita, Scripta Mater. **65**, 974 (2011).
[103] H. Razavi-Khosroshahi, K. Edalati, M. Arita, Z. Horita, and M. Fuji, Scr. Mater. **124**, 59 (2016).
[104] V. V. Boldyrev, Russ. Chem. Rev. **75**, 177 (2006).
[105] F. Delogu, Acta. Mater. **59**, 2069 (2011).
[106] F. Delogu, Scr. Mater. **67**, 340 (2012).
[107] C. Suryanarayana, Rev. Adv. Mater. Sci. **18**, 203 (2008).
[108] L. Takacs, Acta Phys. Pol. A **121**, 711 (2012).
[109] L. Takacs, Chem. Soc. Rev. **42**, 7649 (2013).
[110] P. Balaz *et al.*, Chem. Soc. Rev. **42**, 7571 (2013).
[111] S. Zhao, E. N. Hahn, B. Kad, B. A. Remington, C. E. Wehrenberg, E. M. Bringa, and M. A. Meyers, Acta Mater. **103**, 519 (2016).
[112] R. A. Andrievski and A. V. Khatchoyan, *Nanomaterials in Extreme Environments* (Springer, Berlin, 2016).
[113] R. J. Asaro, J. Appl. Mech. **50**, 921 (1983).
[114] B. Feng and V. I. Levitas, Mater. Sci. Eng. A **680**, 130 (2017).
[115] V. I. Levitas and O. M. Zarechnyy, J. Phys. Chem. B **110**, 16035 (2006).
[116] V. I. Levitas and O. M. Zarechnyy, Phys. Rev. B **82**, 174123 (2010).
[117] V. I. Levitas and O. M. Zarechnyy, Phys. Rev. B **82**, 174124 (2010).
[118] B. Feng, V. I. Levitas, and O. Zarechnyy, Comp. Mater. Sci. **84**, 404 (2014).
[119] B. Feng and V. L. Levitas, J. Appl. Phys. **119**, 015902 (2016).